e-shape

EuroGEOSS Showcases: Applications Powered by Europe

S6P3 – Working Methodology

TABLE OF CONTENTS

1 AIM AND SCOPE

The aim of this document is to provide methodological guideline to achieve the objectives of the products designed in the S6P3 Assessing Geo-hazard vulnerability of Cities and Critical Infrastructures (Fig. 1). The four products are the Interferometric displacement results (1), the Validation report (2), the Active Geo-hazards report (3), and the urban vulnerable areas report (4). Also provide information about the complementary documentation generated during the project that help to apply it over new test sites.

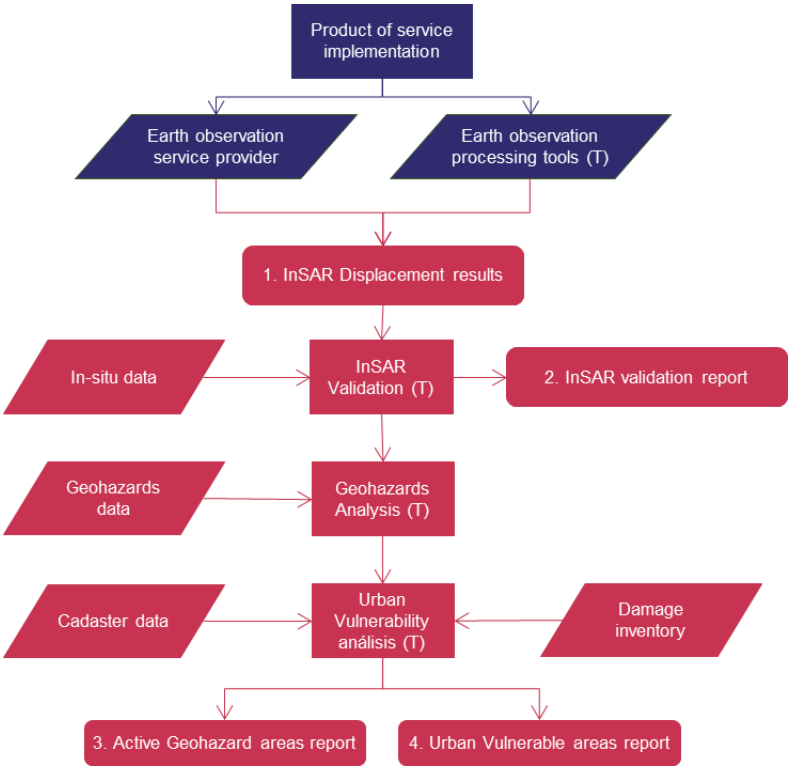

Figure 1: S6P3 Methodology workflow

1.1 Complementary documentation

1.1.1 Test site Requirements

InSAR data are continuously acquired by satellites all over the world. Instead of that, the analysis proposed in this methodology can only be performed if other in-situ and auxiliary data are available. The absence of those data can make the new area unselectable or some of the reports unfeasible to be generated.

All the data required and layer formats are available at the “Data Requirements Report”

1.1.2 Co-design methodology

Direct collaboration with stakeholders is a significant step in this methodology since the most interesting analysis are linked to the availability of precise in-situ and auxiliary data. A general guideline to contact and discuss the results with them has been designed and available at the "Co-design procedure" document.

2 INTERFEROMETRIC DISPLACEMENT RESULTS

2.1 InSAR Technique overview

A Synthetic Aperture Radar (SAR) is an active microwave sensor which provides radar images at high spatial resolution. It can be mounted on a spaceborne platform acquiring data regardless of the weather. These spaceborne sensors operate day and night in a quasi-polar orbit, either ascending (south - north) or descending (north - south). Since the early 90s, several SAR satellites with everimproving imaging characteristics have been launched by an international community of satellite providers, collectively ensuring continuous coverage of the Earth with SAR data (Flores-Anderson et al., 2019). The characteristic bands at which SAR satellites operates are L-band, C-band and X-band, with wavelengths of 23.6, 5.6 and 3.1 cm, respectively. With moderate- to high-resolution capabilities and increased vegetation penetration, C-band data can be seen as a good compromise between Xband and the longer wavelength L-band sensor classes to monitor areas with low to moderate vegetation.

Among the C-band spaceborne sensors, the Sentinel-1 (S-1) mission from the European Space Agency (ESA) comprises a constellation of two polar-orbiting satellites that were launched in 2014 (Sentinel1A) and 2016 (Sentinel-1B). They are expected to transmit Earth observation data for at least 7 years and have fuel on-board for 12 years. Two other spacecraft (Sentinel-1C and Sentinel-1D) are planned to replace the first two satellites at the end of their operational lifespan. Since 2022 Sentinel-1B satellite suffered damages ceased to provide new images reducing the acquisition frequency to 12 days until its replacement by the new sentinel generation (1C-1D). The mission is designed to provide enhanced revisit frequency, coverage, timeliness and reliability for operational services and applications requiring long time series. As part of Copernicus, that is the European Union's Earth Observation Programme, the Sentinel-1 mission adopted a free, full, and open data policy to all users for the S-1 data products via Copernicus Open Access Hub (https://scihub.copernicus.eu/)

2.2 InSAR Processing

Satellite radar differential interferometry (DInSAR) is a geodesic technique, with cloud penetrating and day-night operational capabilities, that allows to remote sense small displacements of the terrestrial surface by analyzing the phase differences between pairs of single look complex (SLC) SAR images.

Thanks to the availability of large SAR data archives, a stack of independent interferograms can be created from various SAR images of the same illuminated area. This allows to reconstruct displacement time series from selected point scatterers (PS) or distributed scatterers (DS) that are above a phase stability threshold in all the interferograms, using the so-called multitemporal or Advanced Differential radar interferometry (A-DInSAR) algorithms. Typically, a minimum of 15-20 images is needed to perform an A-DInSAR analysis with C-band (Crosetto et al., 2016). In any case, the larger the number of available scenes, the better the quality of the deformation velocity and time series estimation. There are two methods to create the stack of interferograms. The first one uses a single reference SAR image (Single master) so the number of interferograms will be N–1, where N is the number of SAR images. The second one uses a small baseline configuration, where a denser interferogram network is created linking multiple SAR images (Multi-master). The criterion to select the punctual targets in the interferograms can be simplified in amplitude and coherence methods. Amplitude selection methods work at full resolution and limit the interferometric processing only to those pixels that behave consistently over a long period of time (PS). Coherence based methods use distributed scatters (DS), or in other words, areas whose scatter properties are not altered with time, which requires a multilook that lowers the resolution.

Any A-DInSAR algorithm dealing with data stacks, requires a number of conceptual steps that have to be sequentially performed (Casu et al., 2014). These are the SAR image focusing (if raw data is used, not needed in SLC images), the SAR image co-registration using a Digital Elevation Model (DEM), the interferogram generation, the unwrapping of the computed phases and the retrieval of the final displacement time-series.

InSAR processing is a time-consuming step that must be carried out by experts. In the e-shape framework three options are provided. First, the processing can be obtained from expert InSAR companies available. Second, Geological Surveys can request access to the GEP platform, an ESA's platform that provides user-friendly tools to obtain InSAR displacement results. Last, the displacement results can be obtained from European Ground Motion Service (EGMS), a European resource provided

by de European Environmental Agency based on InSAR data. Three options have in common that take advantage from the free access Sentinel-1 data.

2.3 Alternatives to obtain InSAR data

2.3.1 Processing through a InSAR Company

Companies dedicated to InSAR processing usually develop their own processing software based on PSI or SBAS approaches or use commercial processing softwares. Providing the study area and preliminary knowledge about the expected geohazard is enough to carry out the process and obtain a good InSAR displacements result. Since this is the easier option, it requires budget availability. After first results are received, first steps of product 2 (processing characterization) should be carried out to check the performance of the processing and suggest changes to the company if the results do not achieve the requested quality.

2.3.2 Processing by GS experts using cloud computing platforms.

Geohazards Exploitation Platform (GEP) (https://geohazards-tep.eu/#!) is a virtual work environments initiative from the ESA. SAR data, processors and computational resources are provided through one coherent interface, allowing users to perform fast and straightforward SAR processes to produce surface deformation mean velocity maps and time series in an unsupervised manner, specifically addressed to scientists that are non-expert in DInSAR data processing.

Access to the platform must be required providing a short project that shows the study area, requested tools, and expected results. Once accepted, the tools are available and a specific budget for processing allocated. For a long-term use of the platform different modalities of payment are being implemented since the service is changing to an economic exploitation model.

Currently two tools are available and functional for InSAR processing: P-SBAS and SNAPPING. P-SBAS processing chain provides a parallel computing solution (Casu et al., 2014; Manunta et al., 2019) for the SBAS approach (Berardino et al., 2002) and it was developed to handle massive SAR archives from current satellites. SBAS uses small baselines to limit the spatial decorrelation, multilooks data to reduce phase noise and applies a coherence-based pixel selection criterion. The multilook applied is 5 x 20 (azimuth x range) which generates pixels in the size of about 90x90 m. This tool was integrated into GEP by CNR-IREA (De Luca et al., 2015). SNAPPING is a solution, recently added to GEP by the Aristotle University of Thessaloniki (AUTh), the research group Microgeodesia Jaén (MJaen) and Terradue s.r.l., that combines the capabilities of SNAP (Veci et al., 2014) to generate the interferogram stack and

StaMPS (Hooper et al., 2012) to generate mean velocity maps and time series. SNAPPING uses a single master interferometric processing approach compatible with StaMPS PSI methodology, an amplitude dispersion criterion for initial pixel selection and the option to apply atmospheric filters (Foumelis et al., 2021, 2018).

Both tools are easy to operate following the next steps:

1- Draw the area of interest.

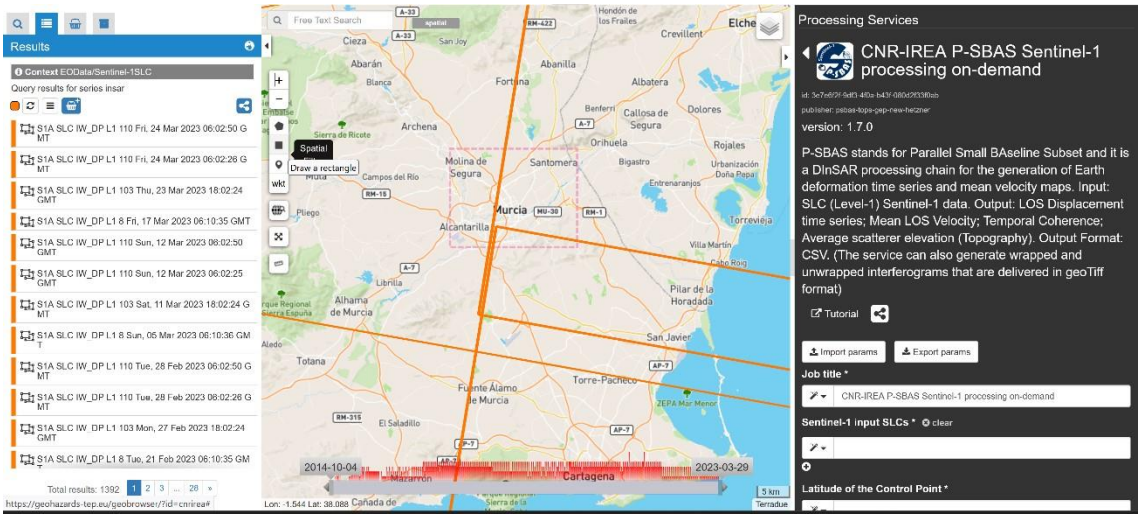

2- Check the available tracks (only one can be selected): Select those which better over the AOI

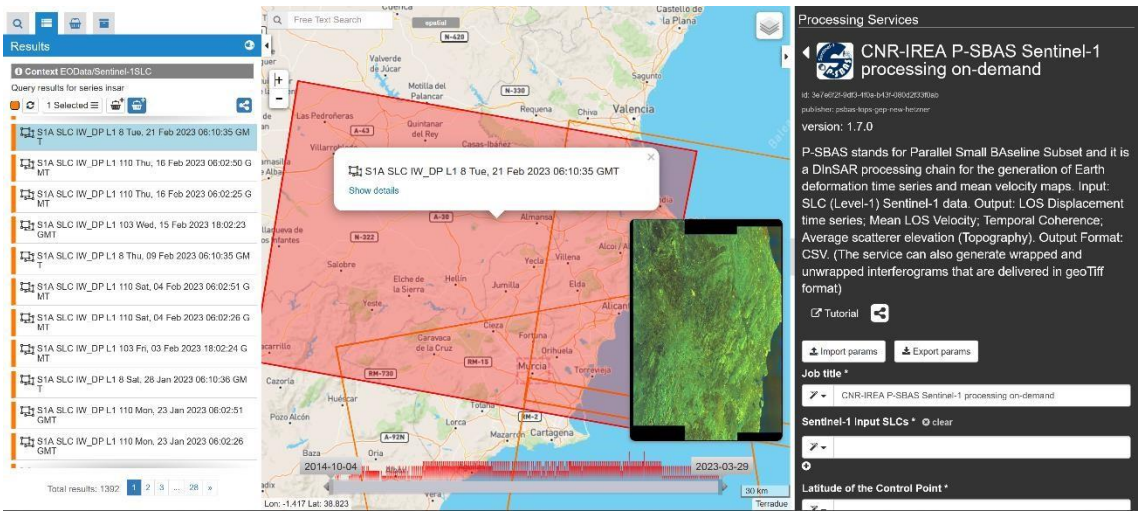

3- Change the filters to improve the selection: Dates, Track

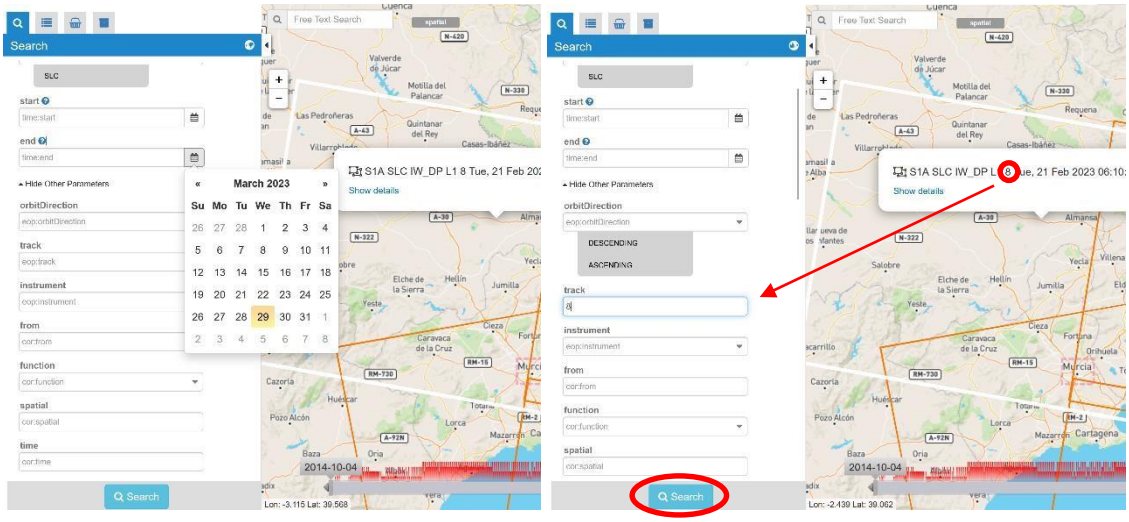

4- Drag the selected images to the processing area

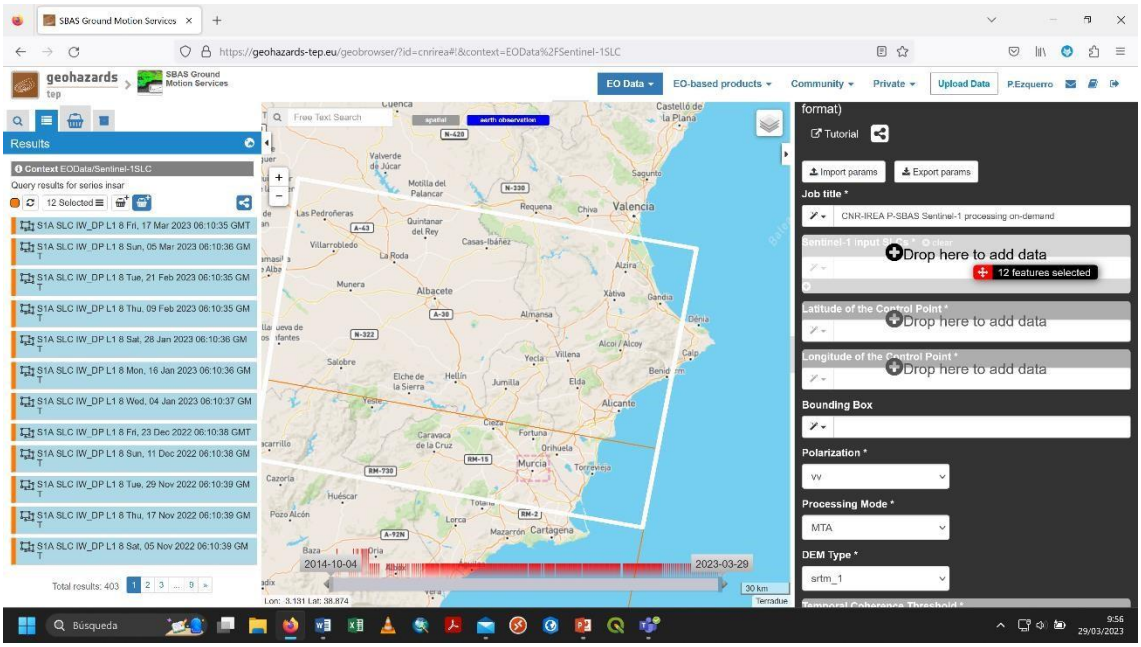

5- Set the AOI (Update the Bounding box with the selection rectangle coordinates)

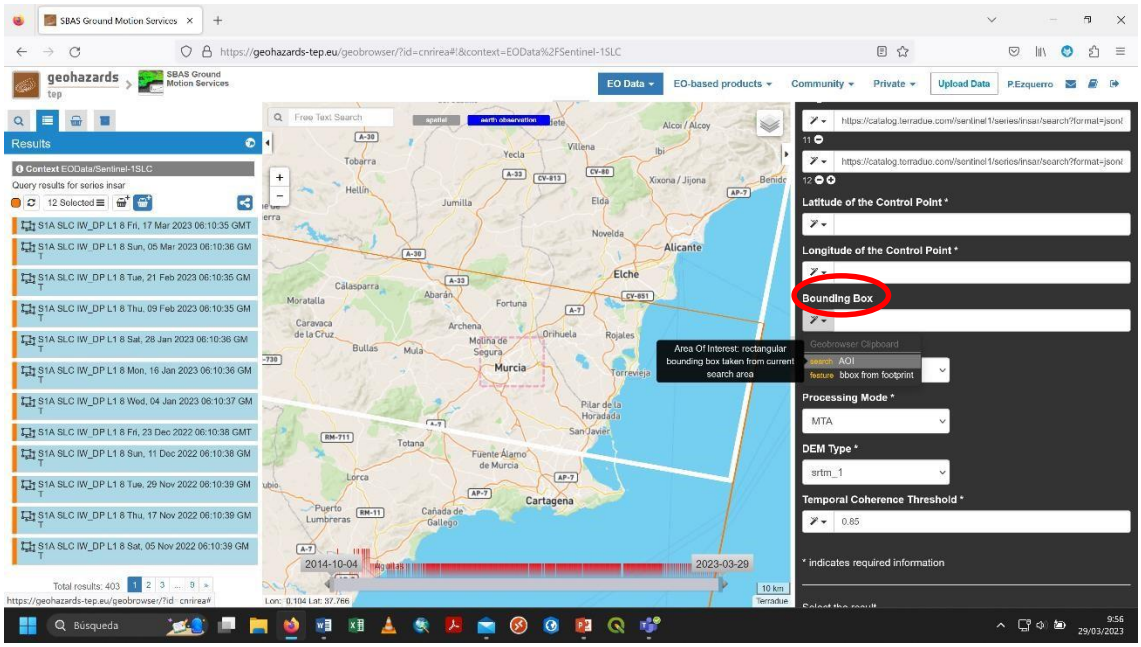

6- Set the stable area: Previously the experts in the area must locate an area (The best option would be a populated area) without displacements associated with the studied phenomenon.

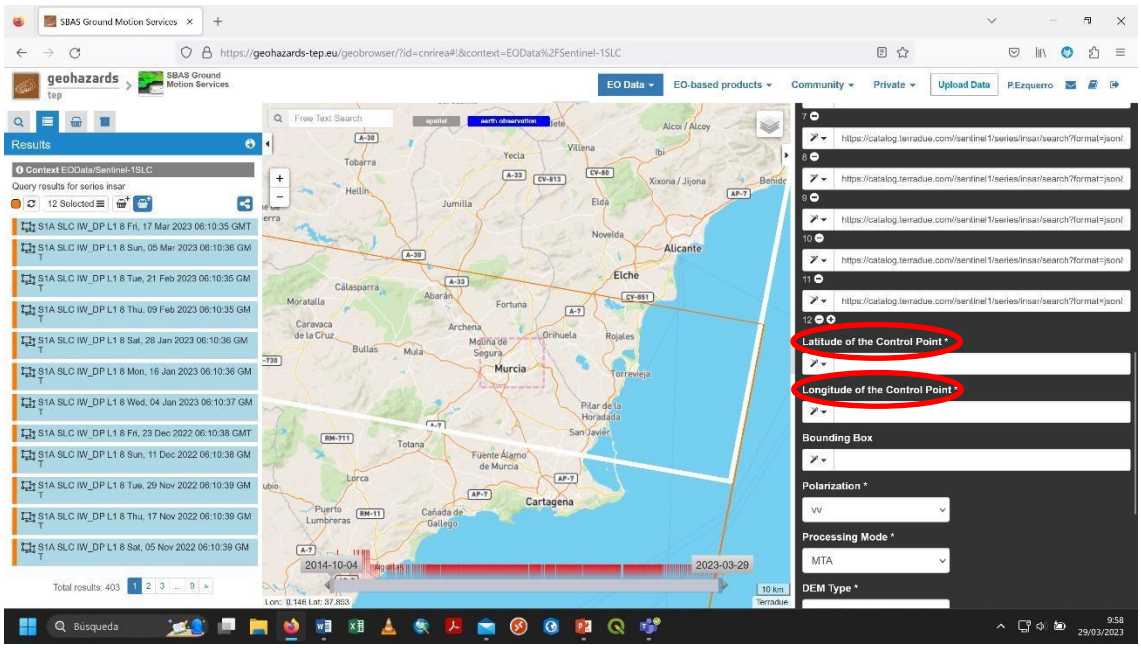

7- Launch the process.

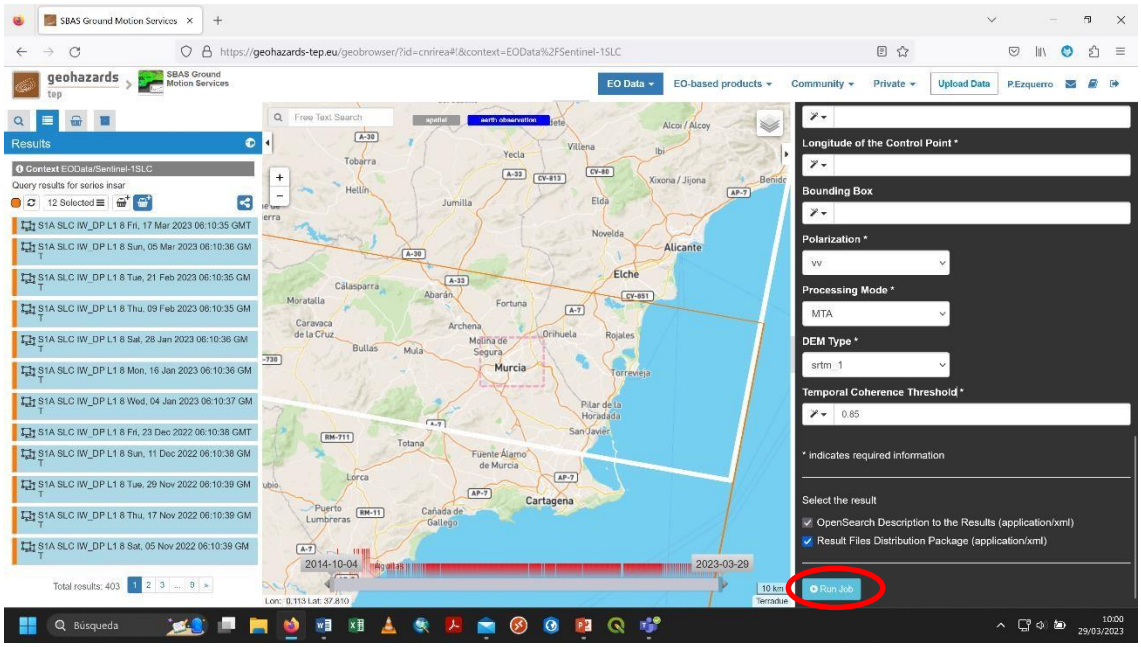

8- Download the results in an .csv file for ongoing work.

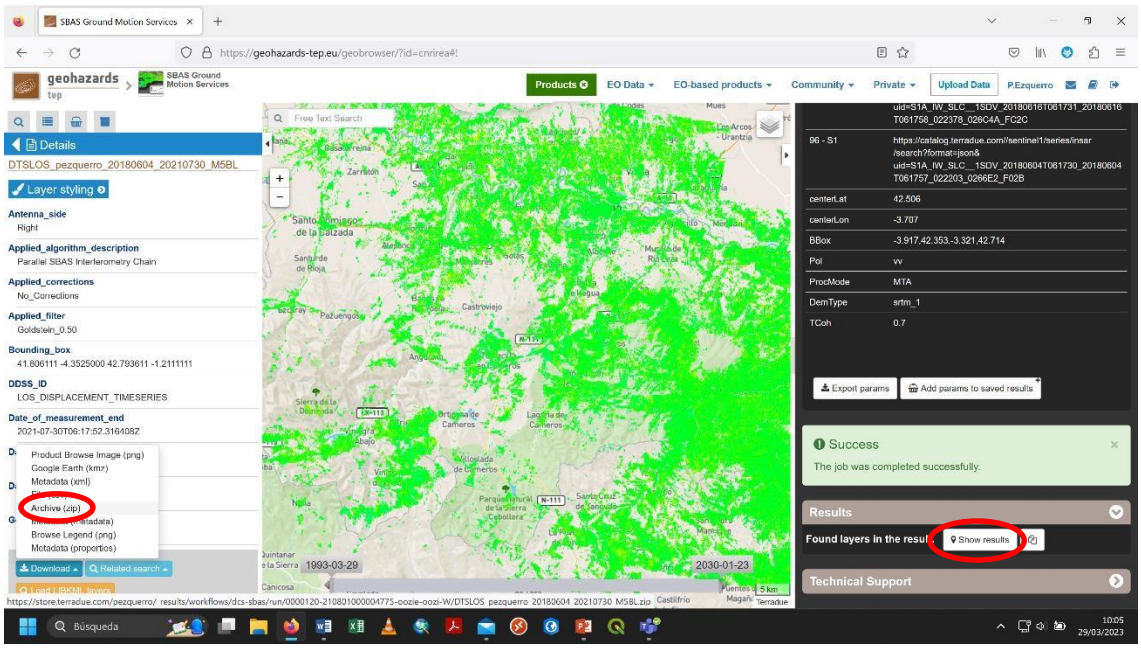

Last, it must be said that the results obtained using these tools must be validated since are the output of an automatic process and can be affected by several uncertainties. Validation will be explained in the validation section.

2.3.3 European Ground Motion Service

EGMS results provide Line of Sight (LOS) displacement at full resolution (5x20m) for all the European area. These data are free available to download at the EGMS website (https://egms.land.copernicus.eu/). This is the best option to obtain preliminary results and know the InSAR problems related to a specific location. EGMS results are processed as a massive process and must be validated over the selected AOI to carry out further analysis. Since the beginning of 2023 the processed period available is 2015 – 2021. A yearly update is expected covering a period of 7 years (i.e. next release will cover the 2016 – 2022 period) in order to reduce the propagation of errors in long time series. Previous versions will remain available.

Steps to download the EGMS results:

1- Search the AOI and select the basic product (full resolution). Needs free registration

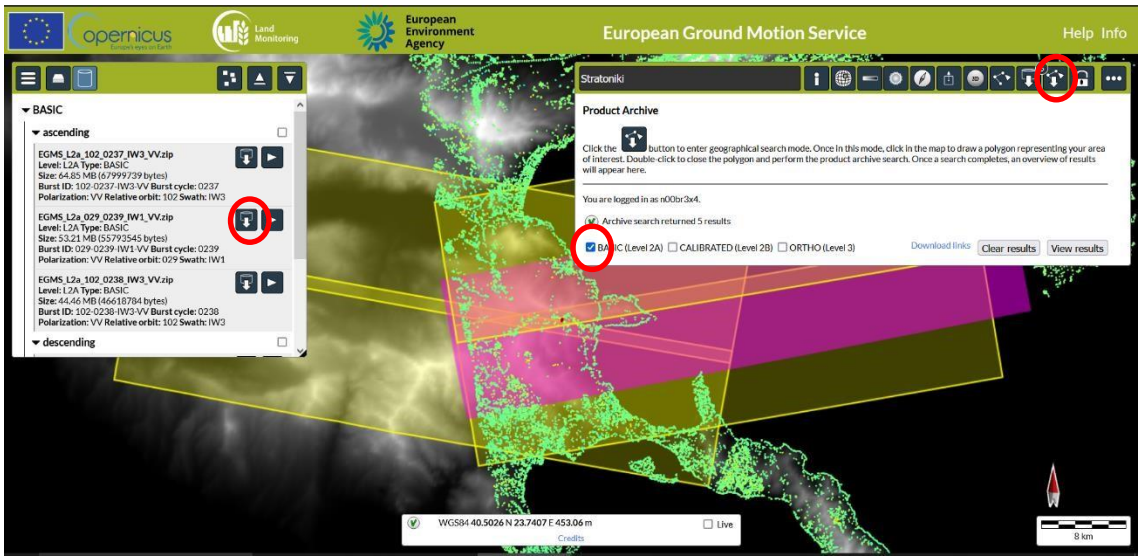

3 INSAR VALIDATION REPORT

InSAR data are widely used to determine the displacements of several natural and anthropogenic phenomena. Despite their consistency, they are affected by multiple sources of noise that difficult their analysis, specially if they are around the detection thresholds. These facts make validation a necessary step for further analysis, moreover in the case studies where no InSAR works were previously done. InSAR validation report provides information to perform a validation analysis depending on the available in-situ data and monitoring data (Fig.2).

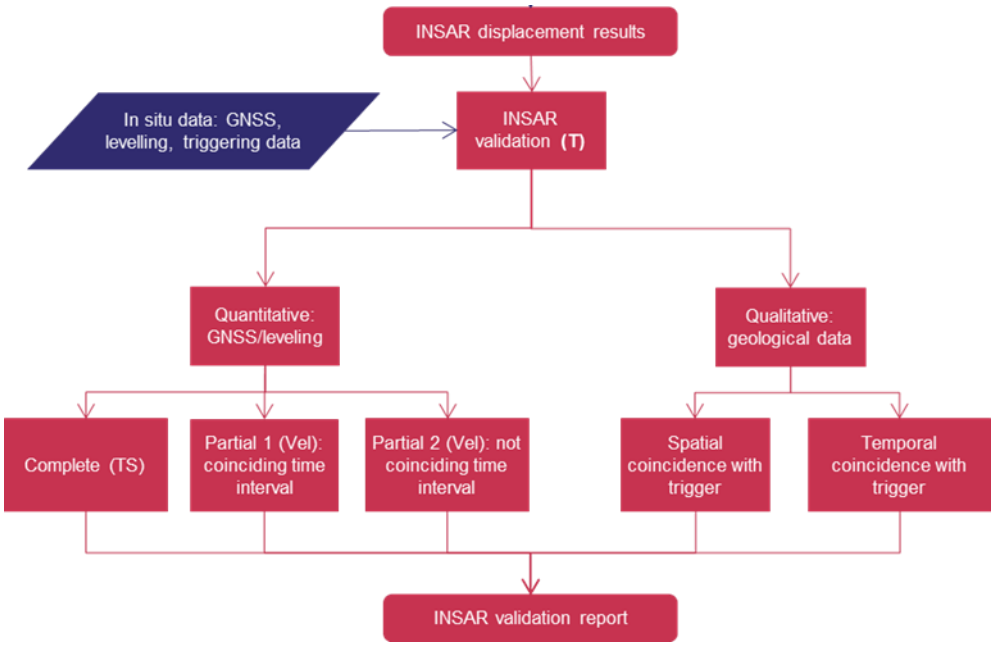

Figure 2: Validation methodology based on quantitative and qualitative solutions

3.1 Quantitative Validation

Optimal validation of InSAR Data is the spatial and temporal comparison of displacements with other monitoring data as leveling, GNSS stations or other InSAR data. These data are usually difficult to obtain, moreover if they have to be temporarily coincident. In order to provide a validation result, three levels of validation are defined with decreasing level of confidence.

Level 1 validation (Complete) requires monitoring data with available time series and major overlapping of sensing periods. The information provides from supplementary InSAR data (different sensor or processing chain is recommended) or GNSS permanent stations.

Level 2 validation (Partial 1) is selected when only displacement velocities are available, and dates overlap. This information is provided by leveling and GNSS measurement campaigns. Also, some InSAR products that only provide displacement velocities are a source of data for this validation level.

Level 3 validation (Partial 2) could be explained better as a comparison of velocities over the same are but in different temporal period. It is between quantitative and qualitative validation because only allow to analyze if the phenomenon continuous a similar trend or dimensions. Al sources of monitoring data can be used in this level.

3.1.1 Validation methodology using punctual data: GNSS data.

InSAR measurement points are representative of the resolution pixel selected, not only the point represented (which is the centroid of that pixel). Also, a singular InSAR point is not representative by itself and must be coherent with the surrounding ones. In order to validate the results, the mean displacements of all the points around the GNSS station must be calculated. Usually, a 100m buffer around the point is enough to obtain at least 6 to 10 points (Fig. 3). Increase the radio until the number of InSAR points reach that number to obtain a consistent result.

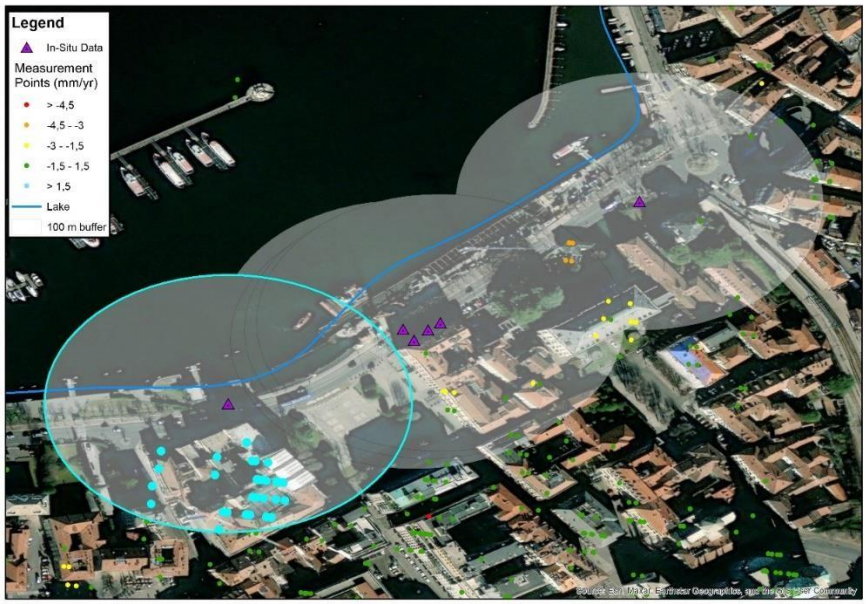

Figure 3: Quantitative validation example. All the INSAR measurement points within the in-situ data buffer (light blue) are selected for validation.

Once the time series are obtained both time series have to be adjusted to the same dates, selecting the dates with InSAR data from the daily GNSS records. Usually, a 15-day mobile mean is applied to the GNSS data to reduce the signal noise. In order to compare both series R^2 and Root mean square error (RMSE) are calculated and validation accuracy (Fig. 4) obtained from Navarro-Hernández et al. (2022). Note that RMSE values must be divided by the stability threshold to obtain the relative RMSE

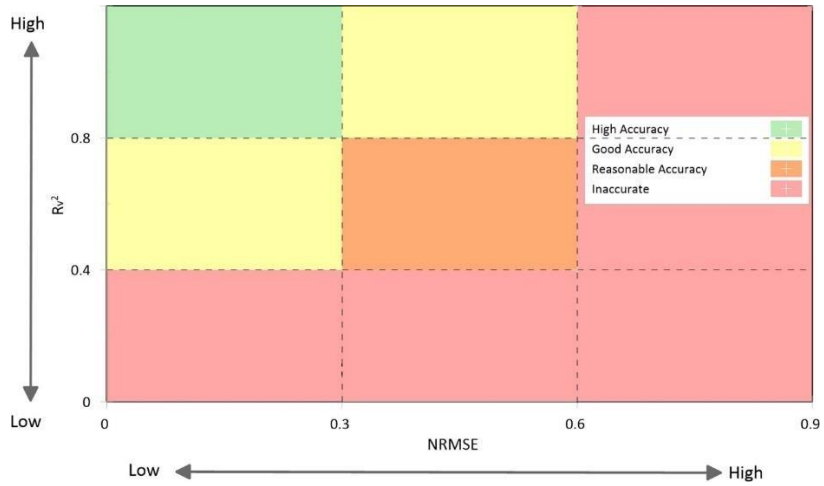

Figure 4: Accuracy matrix proposed by Navarro-Hernández et al. (2022)

In the case of validation levels 2 and 3, time series are not available. In those cases, the buffer methodology is applied in the same way, selecting no less than 6 measurement points. Velocities from similar periods can be directly compared (Level 2) obtaining the errors. Using several validation points, spatial R^2 and RMSE can be calculated, and validation accuracy obtained. If the periods are not the same only a comparison of the velocity can be achieved (Level 3) using auxiliary data to understand their possible differences.

When the results of the validation are in the first three classes of the accuracy matrix, the validation can be considered as correct. If the validation is considered as inaccurate, the reasons can be problems related to the processing or the reliability of the in-situ data. Magnitude discrepancies could suggest different accuracy of the measurement devices or problems related to the geometry of the surface (i.e. orientation with respect to the satellite LOS). Spatially generalized differences, like ramps or general trends would be probably generated by problems during the processing and it should be refined. This interpretation of the validation results is similar when working with two InSAR datasets (section 3.1.2)

3.1.2 Validation methodology using distributed data: Two InSAR datasets available.

If two InSAR datasets are available with an overlapping temporal period, a Level 1 spatial and temporal validation can be achieved.

Figure 5: Example of spatial validation of velocities. Pixels without InSAR data in both datasets have been removed because the triggering phenomenon is not identified and

Spatial validation requires to generate a validation grid. The new grid pixel should include around 2-4 measurement points from each original dataset. Original data are resampled to the new grid calculating the mean velocity and time series. Those pixels without data in one of the datasets are discarded for validation. Using "active" pixels the spatial R^2 and RMSE can be calculated with its respective validation accuracy assessment (Fig. 5). Also, spatial distribution of the differences can be obtained to detect possible problems related to the processing. When the trigger of the displacements is a smooth and continuous process like land subsidence, and a regular density of InSAR data available, the interpolation of the results is feasible and generate results easier to visualize and analyze.

Temporal validation can be performed over points of interest or random locations applying the same methodology described for punctual data.

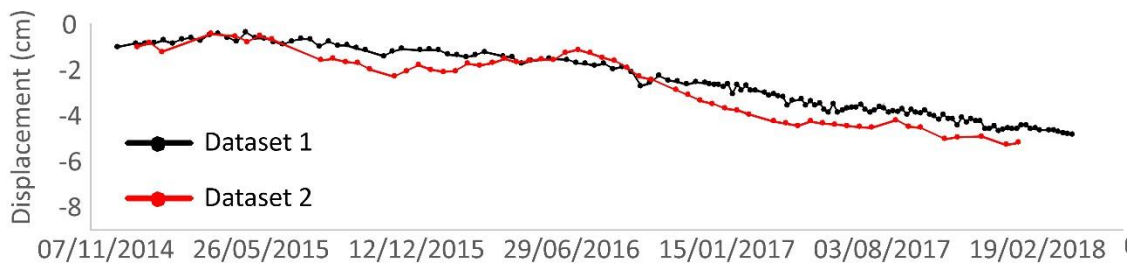

Figure 6: Example of Time Series validation

3.2 Qualitative

In situ data and monitoring data are difficult to obtain in several study areas because they have been recently detected. In that cases direct validation is difficult to achieve and only a qualitative interpretation of the displacements based on auxiliary can be obtained. This kind of validation is especially important over areas with displacements near the stability thresholds, which only can be analyzed joint with this auxiliary data. Specific layers are important for qualitative validation of the different geohazards (Tab. 1)

Table 1: Proposed layers for qualitative validation

Geohazard	Spatial validation	Temporal validation
Subsidence GW changes	Location of wells, Thickness of compressible materials	GW changes
Landslides	Damage detection/displacement evidence, Slope	Pluviometry
Mining activities	Mining works map	Extracted volumes

3.2.1 Spatial Validation

Auxiliary data that represents the location of the phenomenon that is supposed to be generating the surface displacements is compared with the deformation pattern detected with InSAR. As an example, subsidence due to groundwater extraction can be compared with the location of the active wells, subsidence related to mining activities should be related to the mining works (Fig. 7).

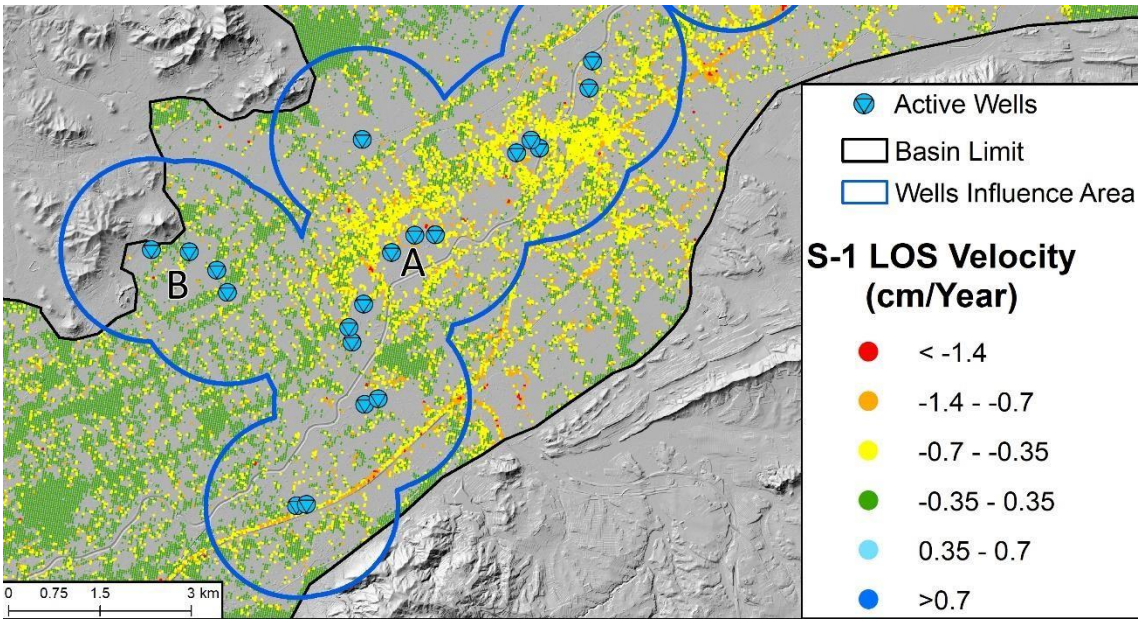

Figure 7: Example of spatial validation. The main displacements are spatially related to the possible trigger.

3.2.2 Temporal validation

Same type of analysis can be done using temporal data. A good agreement between both time series reveals a possible relationship between the InSAR displacements and the auxiliary data.

Good examples are the distribution of groundwater changes during a period, or the volume of material extracted from a mining district between two dates.

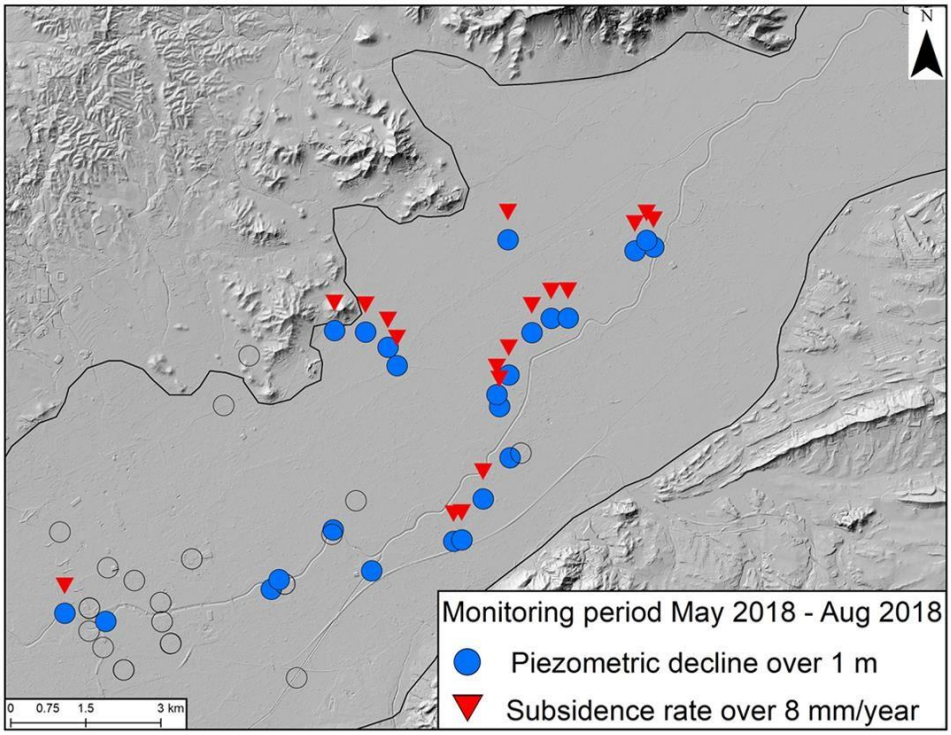

Figure 8: Example of temporal validation. Piezometric and land subsidence trends reveal a coherent trend in most of the area of study

4 GEOHAZARDS ASSESSMENT

This section describes different analysis designed to characterize the main geohazard affecting the study area. The document shows analysis that can be applied to most of the test sites affected by one of the geological hazards and usually useful for the stakeholders. Despite that, codesign process with a specific end-user can derive to provide a new analysis fitted to their necessities.

4.1 Pre-analysis

This section provides, a general overview about InSAR results, with insights about the technique that allow to improve further analysis, and an easy tool to detect the possible geohazard affecting the area, especially useful for large areas.

4.1.1 Processing Characterization

Even high-quality and accurate data, each processing has different noise and trend characteristics, depending on the satellite, topography, and atmospheric effects. Those problems must be identified to be mitigated or, at least, taken into account during the interpretation.

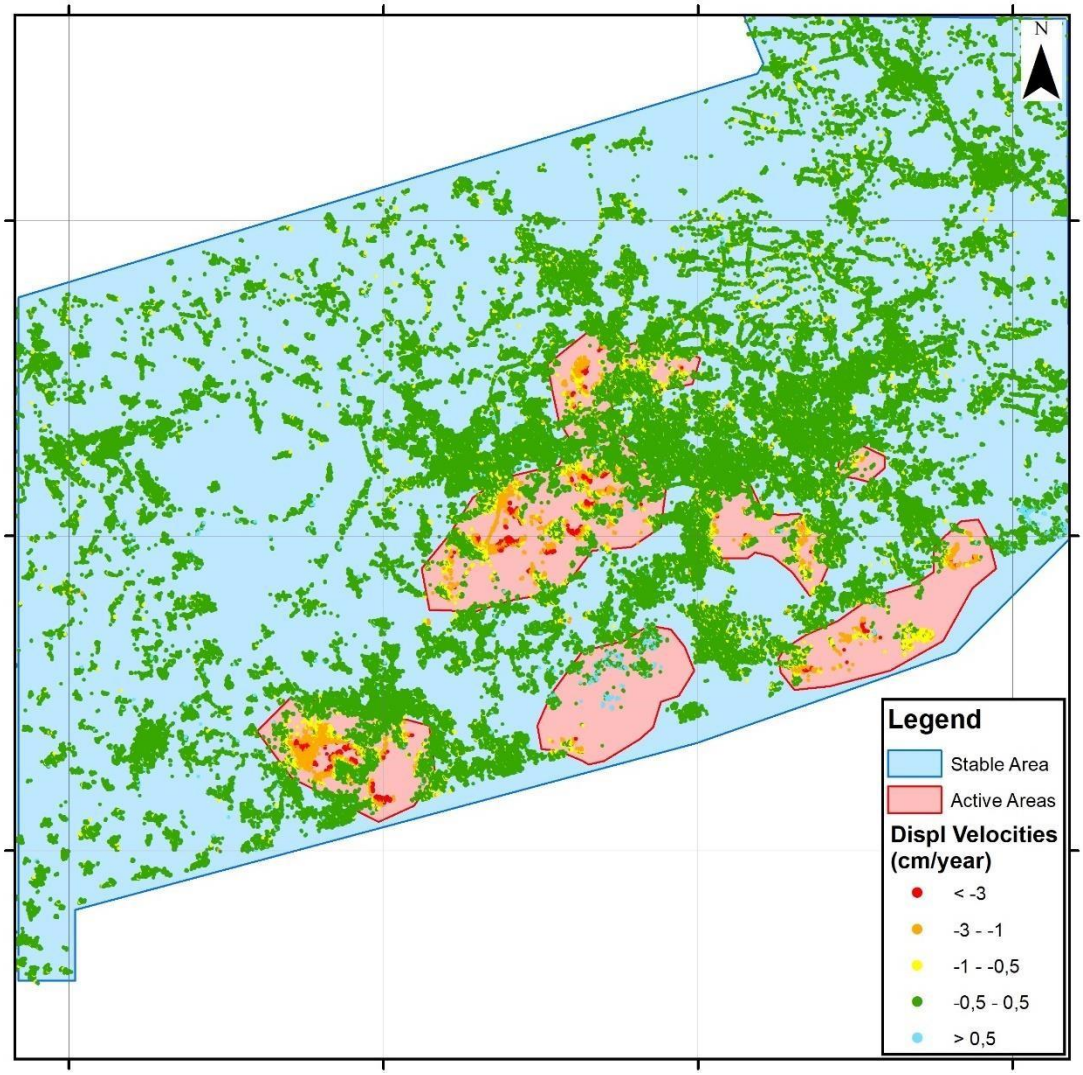

Figure 9: Example of the definition of active and stable areas.

Main parameter is the background noise of the processing. Nominal accuracy of the technique is around 1-2 mm/year, but many areas present larger values due to the above-mentioned effects. First step to define a displacing area is to set a displacement threshold. Before that, a large area where no displacements are expected (i.e. rock material outcrops, urban areas out of a basin) must be defined (Fig. 9). Displacements over that area are supposed to be near 0 and allow to calculate the mean displacement and standard deviation. If the first value is not near 0 probably the area is not stable enough or trend problems are detected in the overall InSAR results. Standard deviation is the key value to find the background noise, usually using between 1.5 and 2 times the std as the stable range (Fig. 10). If the Displacements under that threshold are near undetectable or unanalyzable despite other auxiliary data are available to confirm coherent trends. Same analysis has to be done when working with time series, taking into account that are more sensible to sudden changes due to punctual errors.

In those cases, calculating the stability threshold of the last date provides more robust results.

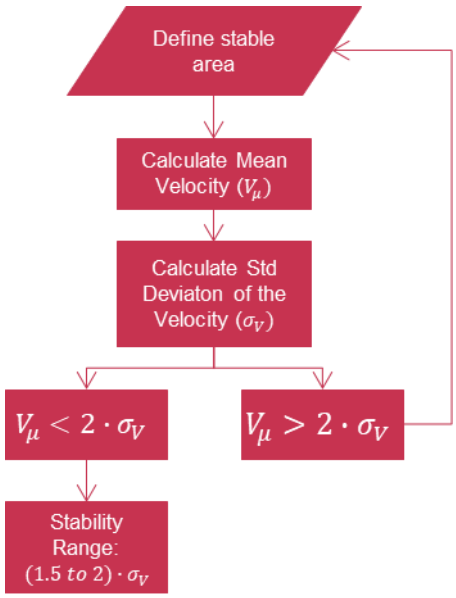

Figure 10: workflow for the definition of a stable area and stability thresholds

Usual stable range values are between 2 and 6 mm/year (Raspini et al. 2012; Heleno et al., 2011). Processings with mean velocity values larger that the stable value can be affected by seed location or other problems related to topography, atmospheric effects or processing errors. First option shows similar mean velocity values overall the stable areas and can be mitigated deleting the common trend. Second type are difficult to resolve and usually needs reprocessing.

4.1.2 Identification of active areas

Medium and small test sites are focused on usually known geological hazards and delimited areas. The identification of the displacing areas is easy once the stable ranges are set. Large test sites with different, disperse and unknown geohazards are more difficult to analyze due to the millions of measurement points obtained with an InSAR processing. Even those are not the main objective of the methodology, some strategies to work with those data are proposed.

Using the mean velocity stable range values, a first selection of the active areas can be done. This selection can be refined only choosing those clusters of points with more than a certain value (Fig. 11). This clustering is useful to obtain a manageable number of areas to be analyzed, but also reduce the problem of isolated measurement points, not representative when using InSAR data. Clustering parameters like number of points and distance to generate a cluster depend on the processing resolution and the type of displacements pursued. Regular distances vary from 1.5 to 3 times the spatial resolution. Also, stability thresholds can be modified with this objective. Looking for a low

e-shape

number of fast and large areas implies distances and stable thresholds on the highest values, while lowest values will reveal more areas but less significant.

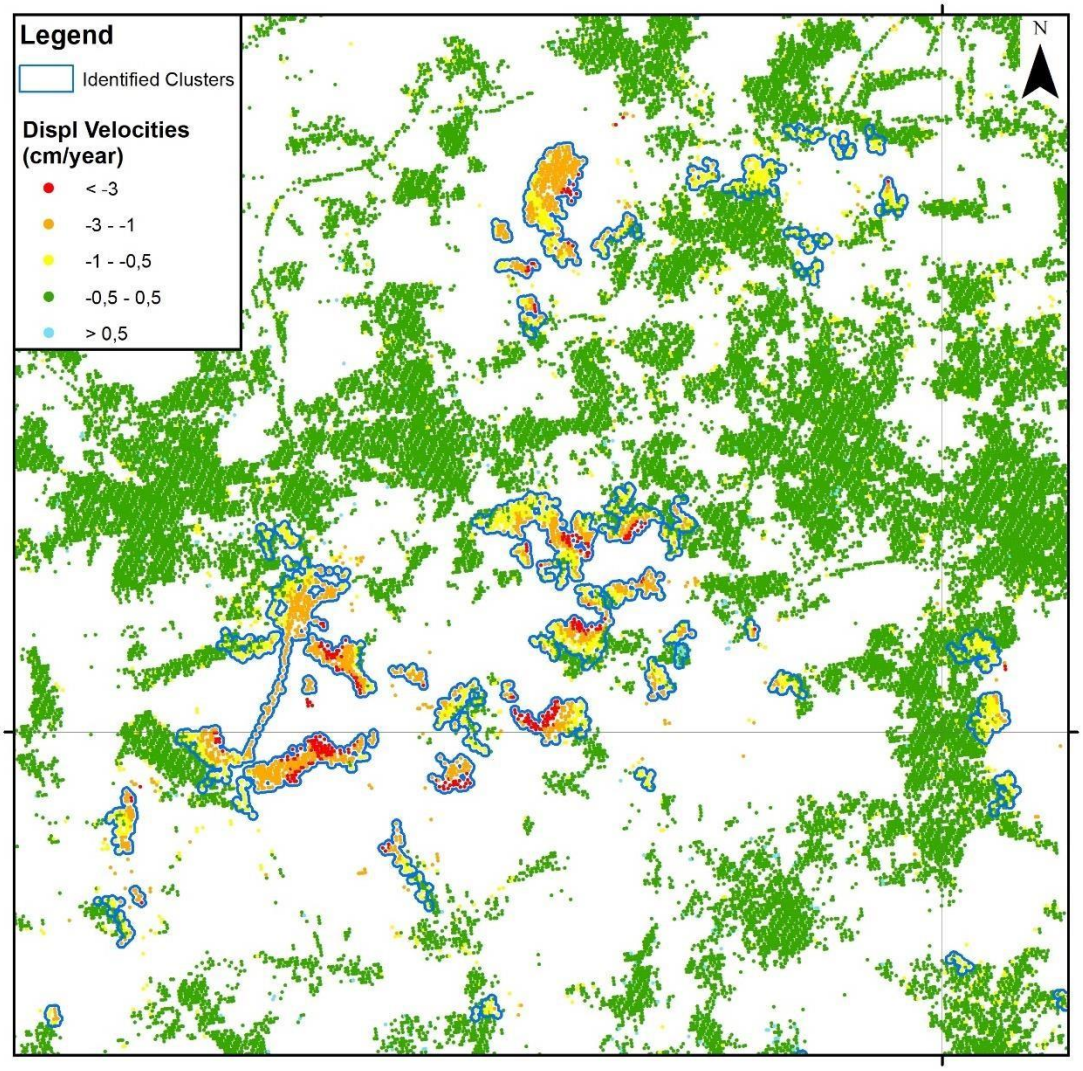

Figure 11: Example of clusters identified. Allow to work with massive data, especially those from automatized processing like GEP or EGMS.

Tools to obtain the results are available in most of the GIS software under the Clustering tags. Specific tools generated to analyze massive InSAR data are also free available for use (Navarro et al., 2018)

4.1.3 Identification of possible geohazard

The identification of the possible geohazard that is generating the detected displacements is more important in those areas with several unidentified displacements. The active areas obtained in the previous step are compared with seven additional information layers, generating as a result of the calculation the possible trigger of the displacements.

The seven layers are Geology, Slope, Land Use, Buildings, Roads and Railroads, Dumping areas, Mining areas and Aquifer systems. In order to facilitate the calculation, the layers can be converted into raster layers and reclassified using the following classes (Numbers of the classes allow to automatize the calculation):

1- Geology: Unconsolidated Sediments (0), Carbonate Rocks (2), Others (1)

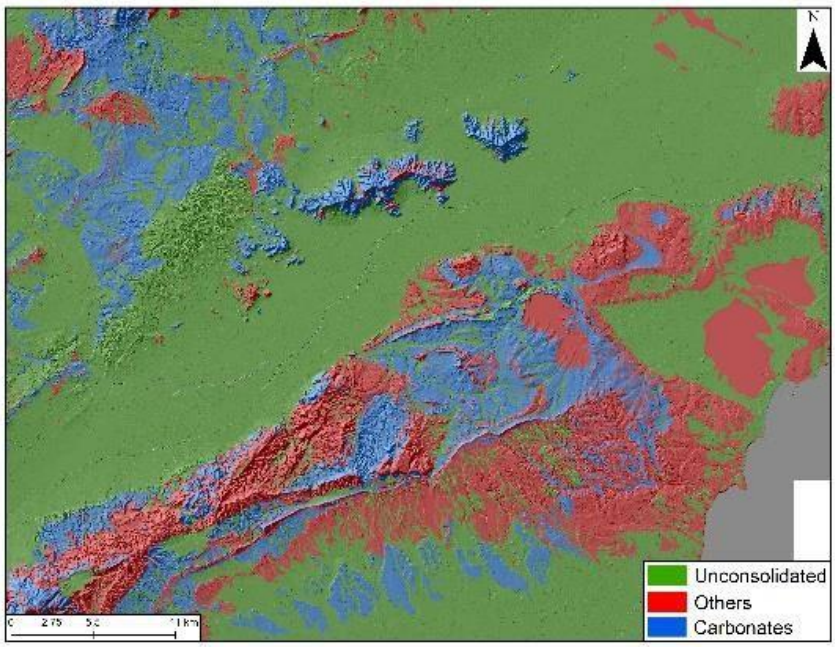

2- Slope: Less than 5% (0), More than 5% (1)

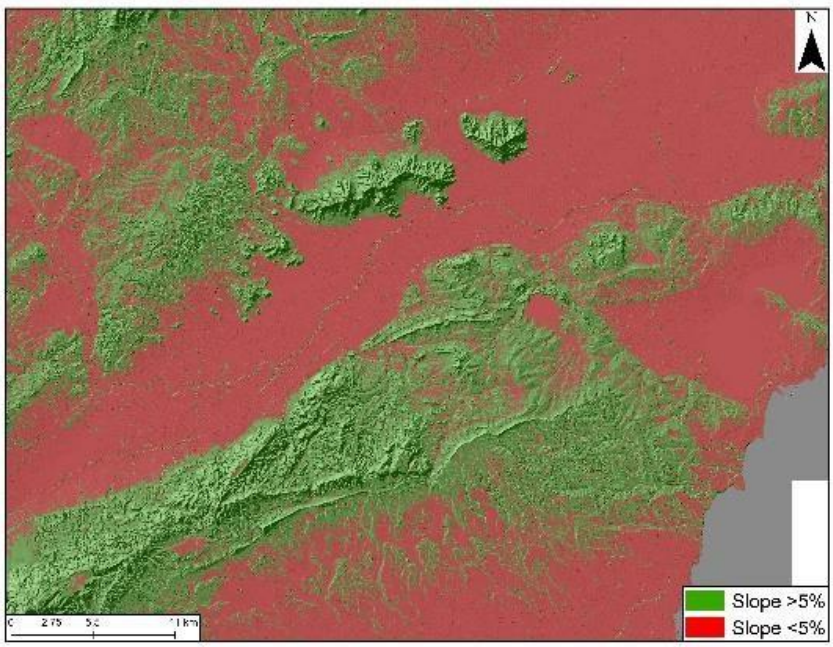

3- Land use: Urban Areas (0), Cultivated Areas (1), Others (2)

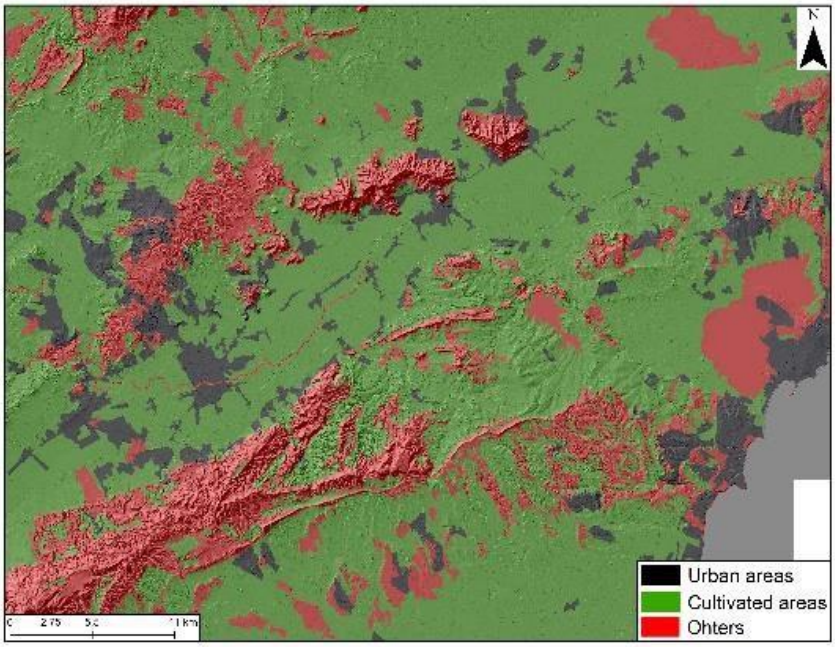

4- Buildings, Roads and Railroads: Buildings obtained from cadastral data. Roads and railroads use a 50 m buffer around the linear feature. The layer is binary, Yes (1) or No (0)

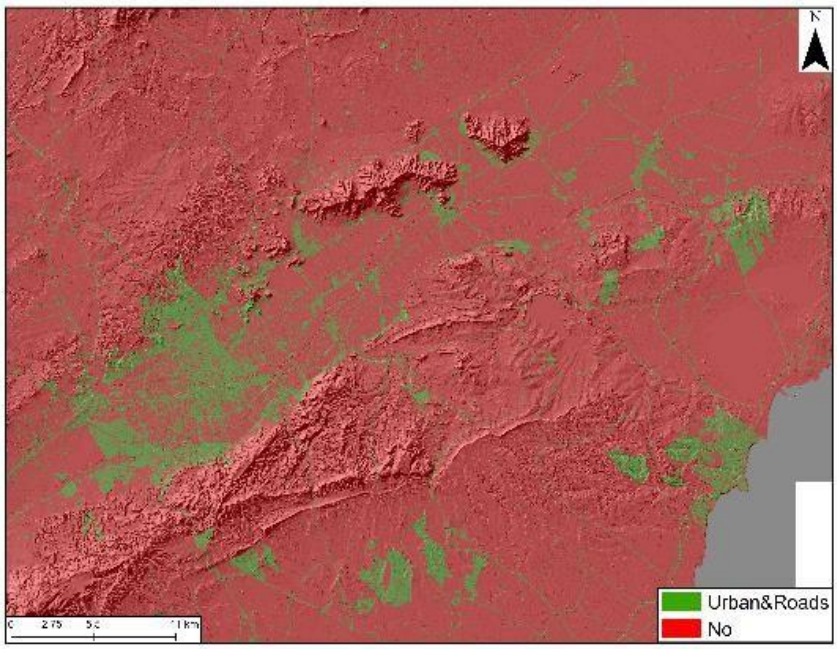

5- Dumping Areas: Dump areas from land use or specific inventories. The layer is binary, Yes (1) or No (0)

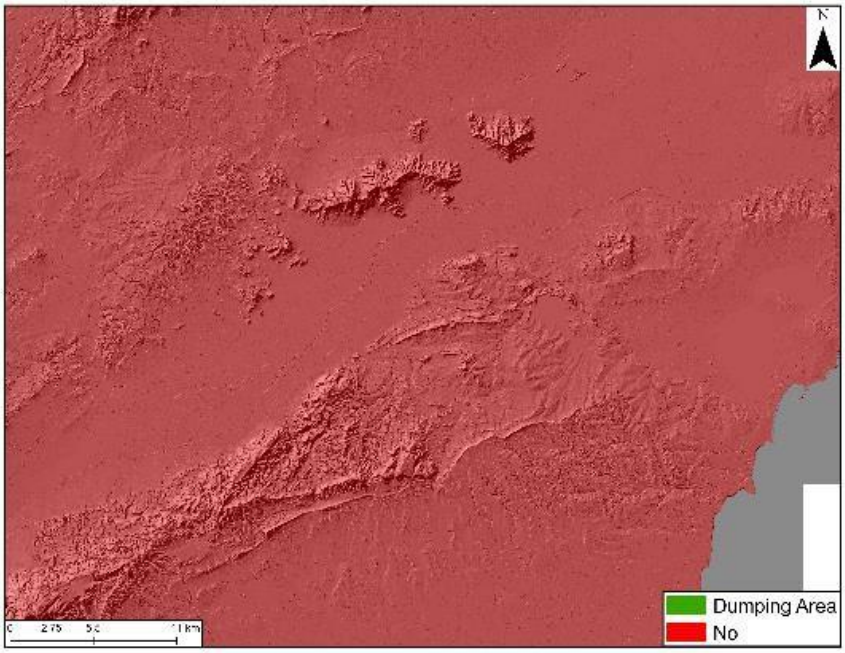

6- Mining Areas: Mining areas from land use or specific inventories. The layer is binary, Yes (1) or No (0)

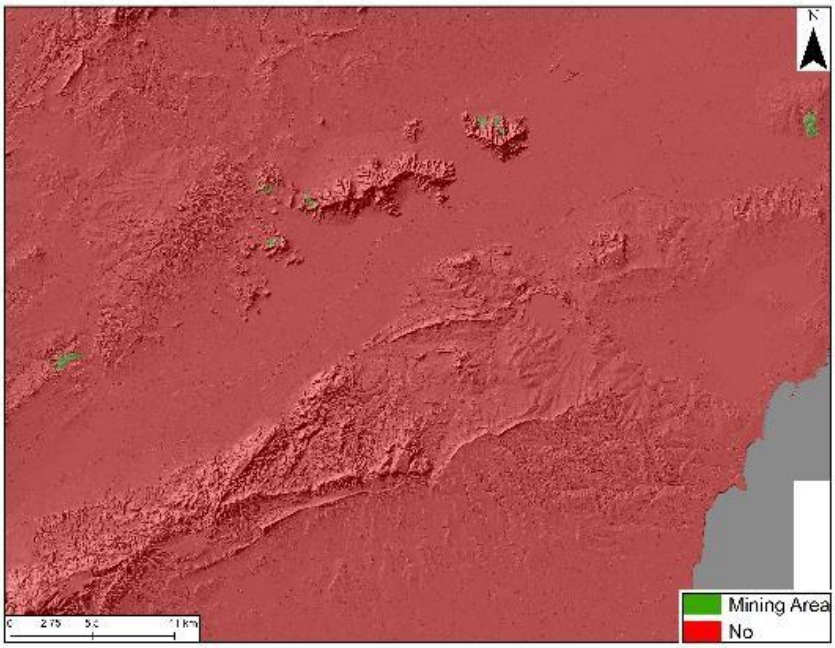

7- Aquifer Systems: Areas with known aquifer-systems. The layer is binary, Yes (1) or No (0)

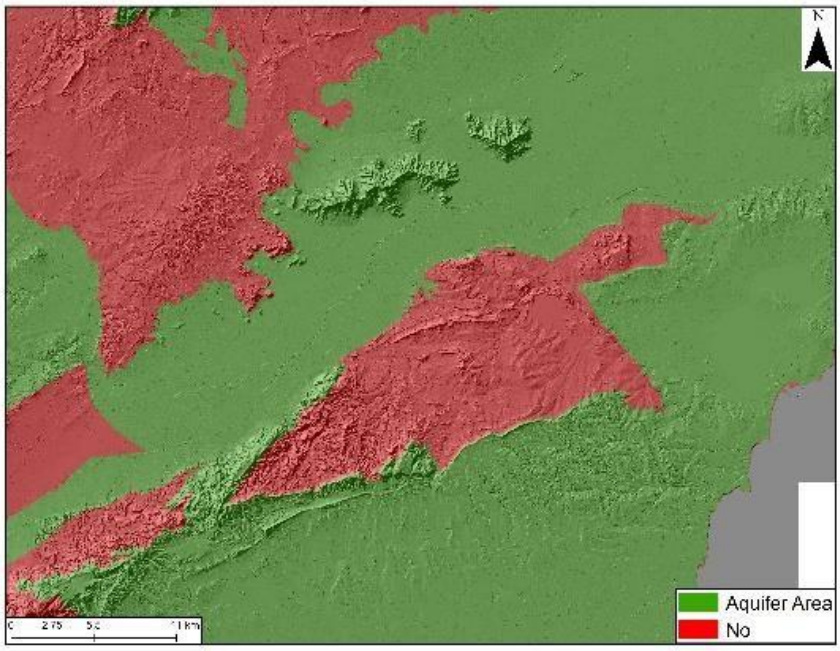

Using these seven layers, seven geohazards can be labelled as a preliminary output: Subsidence due to groundwater withdrawal, Subsidence due to structures and infrastructures consolidation, Landslides, Subsidence due to underground mining, Open pit mining and dump instabilities, Karstic areas, and Solid urban waste (and other) dumps.

The following matrix (Tab.2) presents the classes of each layer that can define each geohazard. "All" tag means that the layer is not significant to define that hazard and all the classes are possible.

Table 2: Geohazards, Input layers and values that define each geohazard

	Geology	Slope	Land Use	Structures	Dump Areas	Mining Areas	Aquifer Systems
GW Changes	Unconsolidated Sediments	< 5%	Urban or cultivated	Yes and No	No	No	Yes
Building / Infrastructure Subsidence	All	All	All	Yes	No	No	All

Landslides	All	> 5%	All	All	No	No	No
Mining Subsidence	All	< 5%	All	All	No	Yes	All
Mining Instabilities	All	> 5%	All	All	No	No	No
Karst	Carbonate Rocks	All	All	All	No	No	All
Dumps	All	All	All	All	Yes	No	No

Extracting the information of the raster layers to each Active Area polygon obtained in the previous section can be done using “Zonal statistics” tools and majority options to determine the class with higher area covered by it (Fig. 12). Calculation of the possible trigger can be also automatized as available in the Excel Appendix B: “Pre_Analysis_Autoevaluation”. Then, the results can be join with the original shapefile using the ID of the polygon, improving the visualization.

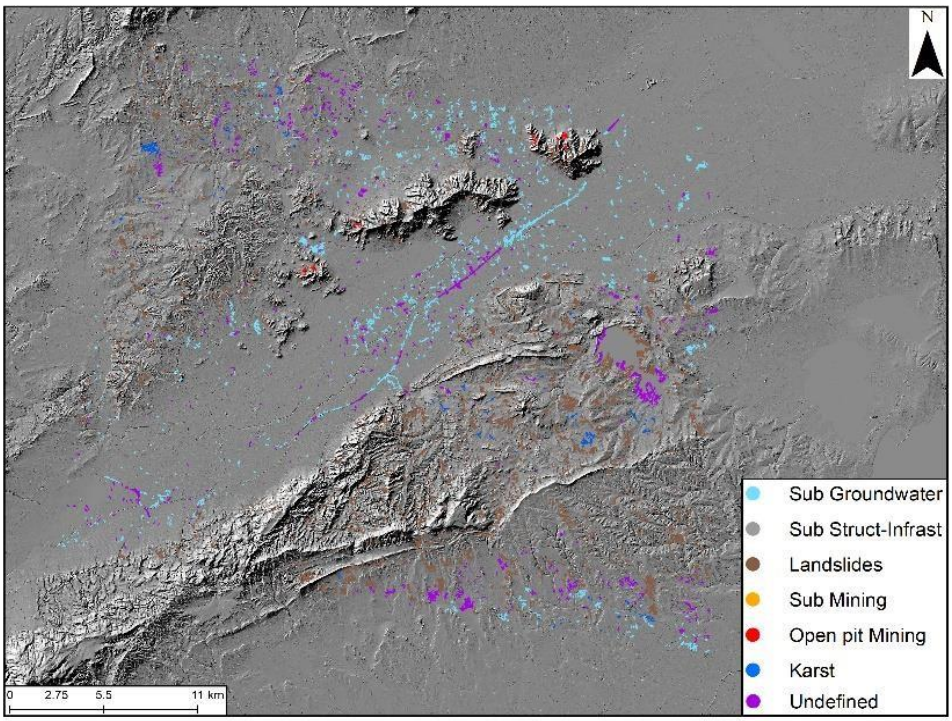

Figure 12: Example of the pre-analysis tool

This is a fast analysis based on general and simplified layers which results have large uncertainties and require a proper validation. Despite that, they can be useful to identify the most interesting areas and improve the analysis of the study area.

4.2 Subsidence due to groundwater changes

Detritic aquifer-systems are subject to changes that modify the pore pressure and generate land subsidence. That subsidence usually has a continuous spatial distribution and smooth patterns. The analysis of this type of geohazard is focused on the delimitation of the affected area and the comparison with the groundwater levels.

4.2.1 Delimitation of the area

The area affected by subsidence is one of the most important parameters for end-users because is a key factor in groundwater management good practices. Taking into account that groundwater levels mainly change due to groundwater extraction, the location of the active wells is very important to analyze de behavior of the study area.

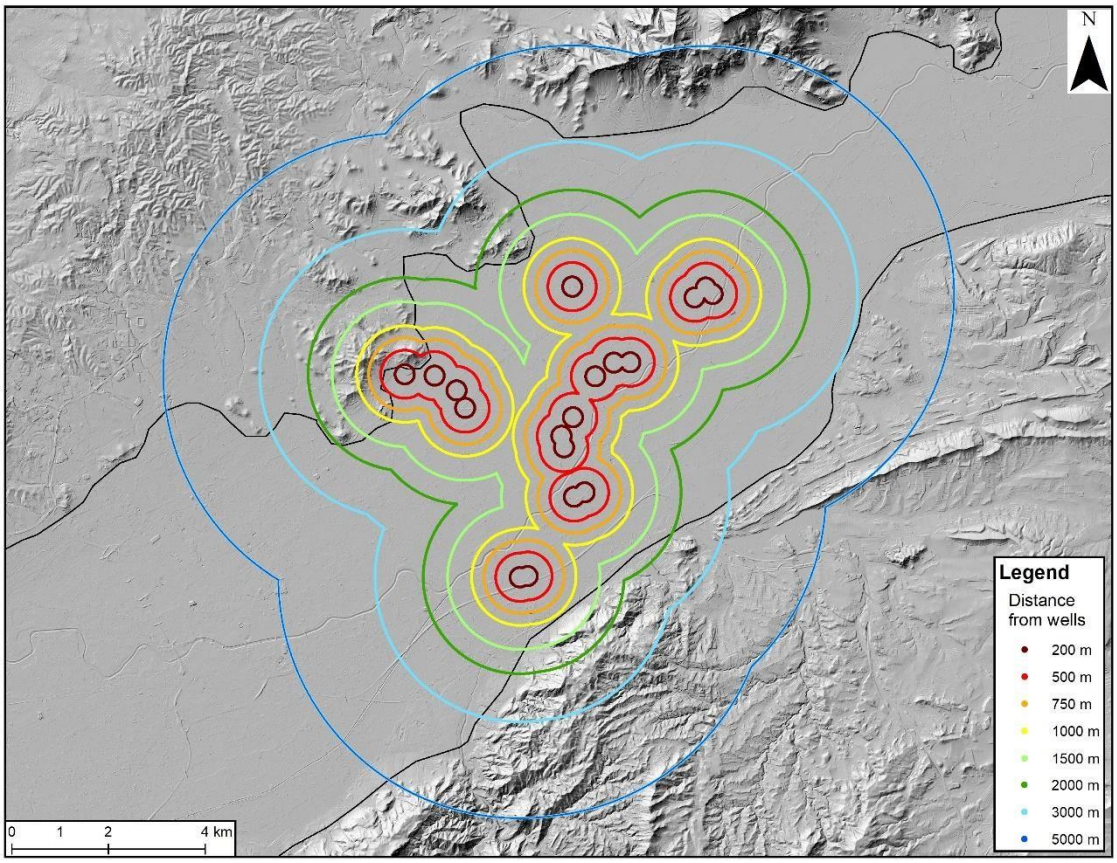

Figure 13: Example of the multiple buffer rings generated to calculate the area of effect of the studied geohazard in relation to the possible trigger

Using the well information as initial point, the spatial analysis requires to generate buffer rings around them. Ring radius can vary from 100 to 500 m depending on the dimension of the subsidence (Fig. 13). The larger ring must cover stable areas. Calculating the main velocity of each ring the spatial pattern of the subsidence can be observed. If the wells are the main trigger of the subsidence, that VelocityDistance curve describes a curve that trends to stability (Fig. 14). Using the stability threshold, the distance where mean velocity is under it can be defined as maximum influence area. Other possibility is to define the influence distance when the slope of the curve is flattened.

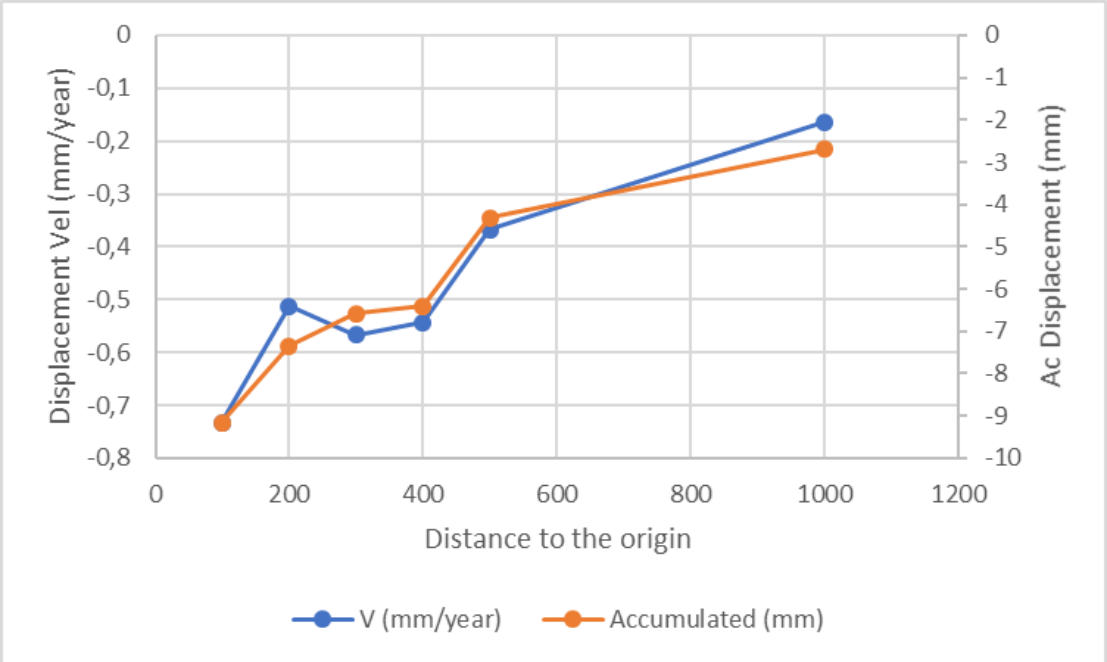

Figure 14: Example of the displacement vs distance results. The inverse relation indicates a possible influence of the studied phenomenon, obscured by the low values detected.

When multiple wells are active in a near area the well field must be jointly analyzed since individual depression cones generate a greater depressed area that distorts the analysis. Depending on the distance between the wells and the continuity of the subsidence this analysis must be done jointly or independently. Moreover, an aquifer system can be affected by periods of extraction and recovery. In those cases, this analysis can be performed for each period using the accumulated displacements and possibly revealing different behaviors that help to manage the groundwater resources. Last, geological variability must be taken into account to understand possible biases in the results.

Figure 15: Example of the "distance of influence" analysis considering other causes than groundwater extraction.

Causes of groundwater changes can be other than extraction, like natural dynamic of the aquifersystems or the influence of near masses of water. In these cases, a similar approach can be used to estimate their possible influence (Fig: 15).

4.2.2 Temporal Behavior

Temporal evolution of subsidence and comparison with the piezometric levels is crucial to understand the possible behavior of the area.

Only attending to the displacement time series, three types of time series are possible (Fig. 16). First (blue) surface displacement subsides during extraction period and recover during recovery ones. This is typically observed in coarse detrital aquifer-systems with an elastic behavior. Second (red), is characterized by a descending trend during extractions and stable periods when pumping is stopped. Plasticity from fine detrital materials prevails and generate a global declining trend. Last behavior (green) corresponds to an aquifer system with a continuous decline of piezometric levels.

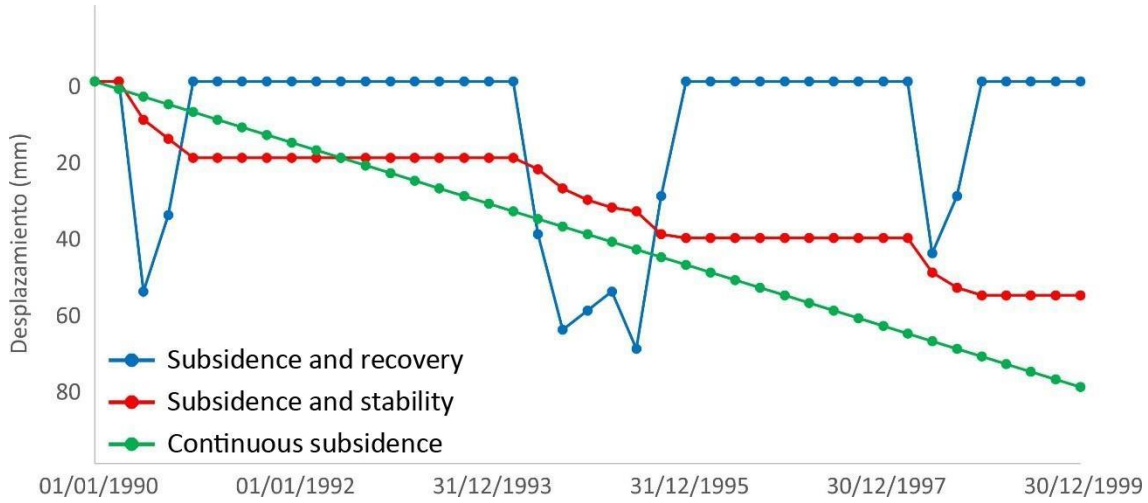

Figure 16: Main type of displacement behaviors observed in areas affected by groundwater changes

It must be noted that temporal period analyzed will influence the analysis. Very short periods that only cover an extraction, recovery or stable period will only provide information about the event and no global dynamics of the aquifer-system. These three ideal behaviors are usually merged in real case studies handicapping the analysis.

Conclusions obtained with the previous analysis can be validated through comparison with the groundwater levels. With dense enough piezometric level records correlation coefficient can be calculated. It will provide a high R^2 if a both time series have similar trends. Another possibility is that a temporal delay exists between groundwater changes and subsidence. That would lead to the existence of clay layers that generate a plastic or visco-plastic response. Many aquifer-systems are very complex, composed by multiple layers of sand lenses interbedded in a clay matrix. In those cases, subsidence is elastic and plastic, elastic when the groundwater changes between previous depths and plastic when the piezometric levels overpass minimum previous levels. The historical data is also important to understand the subsidence dynamics.

Methodologically, all the InSAR measurement points around the piezometer must be selected. As considered in previous sections the minimum number of points must be between 6 and 10. Beginning with a 100 m radio buffer, it can be increased to select the minimum InSAR points until 500 – 1000 m. Then, mean accumulated displacements for each date are calculated, obtaining the mean time series used for comparison.

4.3 Landslides

Surface displacements associated with landslides are spatially restricted by the perimeter of the landslide. This makes them usually smaller than subsidence. On the opposite side, millimetric to centimetric velocities of subsidence change to centimetric to decimetric velocities, or even larger, in the case of landslide. High velocities make landslides easier to detect but damaging. Regarding the feasibility to detect the displacements with InSAR, landslides are located in mountainous areas with different orientations. This will improve or prevent the detection depending on the movement direction.

Taking into account that InSAR satellites have a quasi-polar orbit with around 5-10 degrees of difference with North direction, landslides displacing in that direction are very difficult to detect. If both acquisition geometries are available displacement decomposition can be calculated obtaining the East-West and Up-Down components to improve the analysis.

Decomposition requires to generate a new grid. The new grid pixel should include around 1-2 measurement points from each original dataset. Original data are resampled to the new grid calculating the mean velocity. Those pixels without data in one of the datasets are discarded for decomposition. Using "active" pixels, both components can be calculated with the following formulation (Notti et al., 2014):

$$V_{EW} = \frac{\left(\left(\frac{V_d}{H_d}\right) - \left(\frac{V_a}{H_a}\right)\right)}{\left(\frac{E_d}{H_d} - \frac{E_a}{H_a}\right)} \qquad V_V = \frac{\left(\left(\frac{V_d}{E_d}\right) - \left(\frac{V_a}{E_a}\right)\right)}{\left(\frac{H_d}{E_d} - \frac{H_a}{E_a}\right)}$$

$$H_a = \cos \alpha_a \qquad H_d = \cos \alpha_d$$

$$E_a = \cos(90 - \alpha_a) \cdot \cos(270 - \gamma_a) \qquad E_d = \cos(90 - \alpha_d) \cdot \cos(270 - \gamma_d)$$

Where V is the LOS InSAR velocity, α is the incidence angle, γ the LOS azimuth, and subindex a and d the reference to ascending or descending geometries.

Results obtained after decomposition must be coherent with the slope direction. Problems detected can be due to processing limitations or displacement directions near the "N-S" direction. In those cases, the trigonometric formulation can generate aberrative results due to extreme angles.

4.3.1 Geomorphological analysis

Many landslides, especially those affecting urban areas, are previously delimited and studied. Previous information about geomorphological features is very important for spatial analysis of the

displacements. A geomorphological survey provides information about the landslide header, different lobes, active lobes, distal areas and detected damages (Fig. 17). The faster InSAR velocities will be associated with the active lobes. When no geomorphological information is available, other auxiliary data like DEM and main InSAR data can be used to estimate the morphology of the landslide.

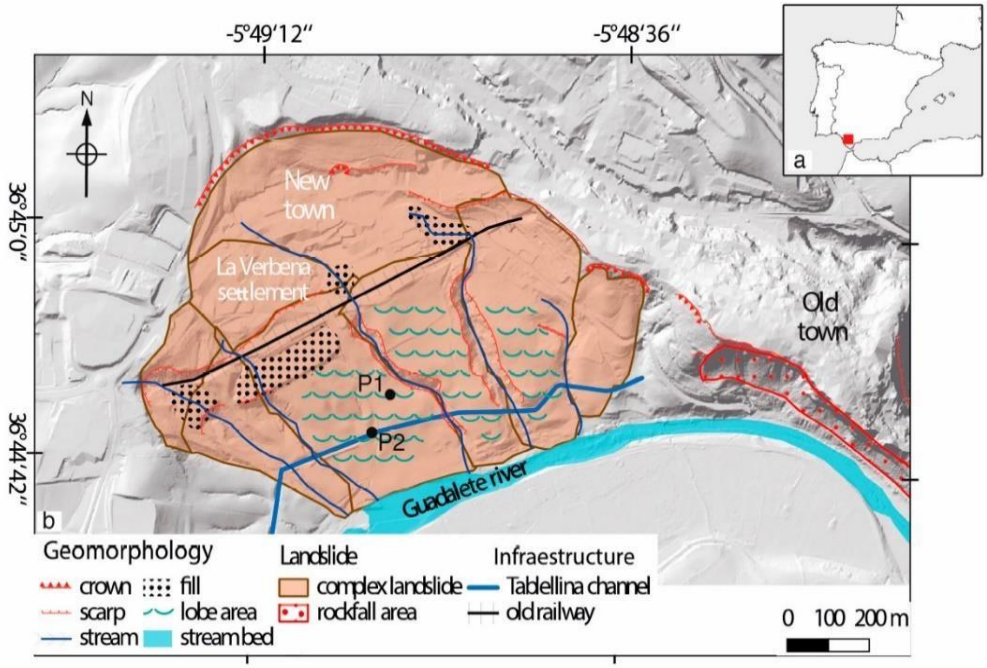

Figure 17: Example of a landslide geomorphological map

4.3.2 Temporal analysis

The analysis of the time series over landslides is a key parameter for the management of the geohazard. Landslides can be stable or active. In the case of active landslides, the acceleration of the displacement can be an early warning because accelerations can trigger a sudden collapse or, at least, a more damaging effect. If a landslide has different active lobes, time series can be calculated over each lobe to detect possible differences.

One of the possible triggers of an acceleration is the existence of a high rainfall episode. A common analysis is to correlate the accumulated rainfall with the displacement time series. Human actions like new structures or infrastructures can also affect the stability of the landslide. Dates and location of those triggers can also be compared with the displacement time series.

4.4 Mining Areas

Mining activity can be divided into open pit mines and underground mines. Problem associated with the first ones are limited to the main pit and surroundings, usually far from urban areas. Geological

e-shape

hazards affecting them are mainly slope collapses in the pit and tailing dumps. The analysis of those areas can be carried out using the same steps than landslides. In the case of underground mines, common problems are related to subsidence due to the mining works. Note that geological materials prone to subside (i.e. unconsolidated sediments) are necessary to trigger subsidence, rocky areas will not probably develop subsidence phenomenon. The most interesting analysis of those areas are to define the spatial affection and temporal evolution.

4.4.1 Spatial correlation

In order to provide a good assessment, auxiliary data about the mining works must be available. The best option is to know the location of the galleries and planned work schedule. With that data InSAR displacements can be compared with the galleries location. The linear layer should be converted into a polygon using a 200 – 1000 m ring buffer and applying the same methodology described for wells.

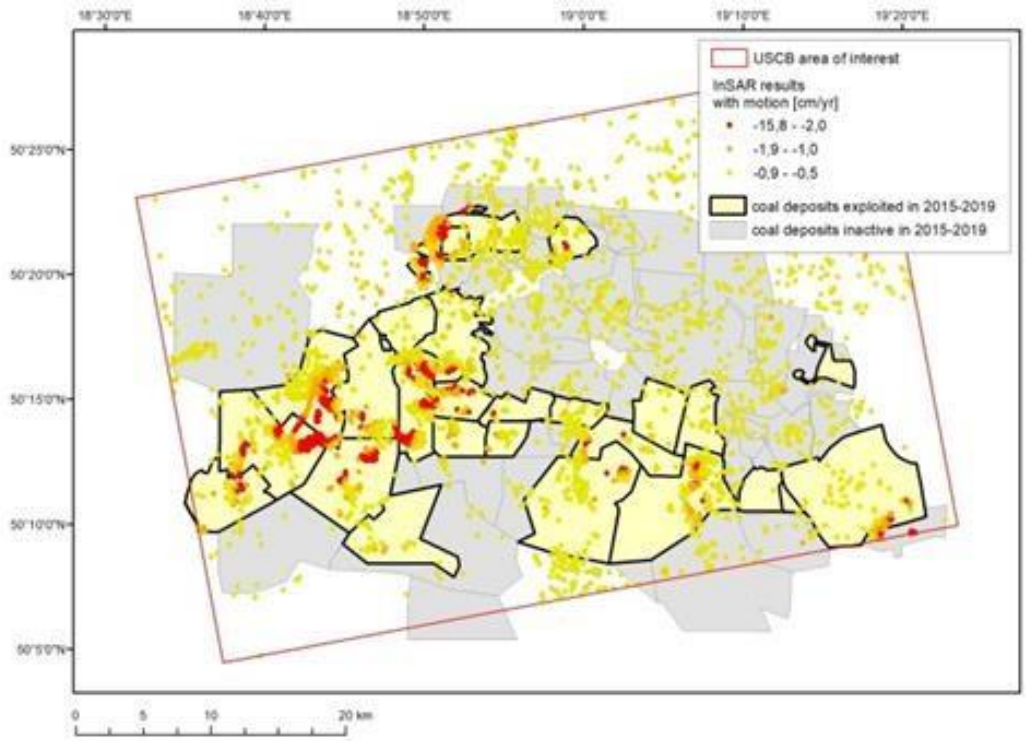

Figure 18: Example of spatial analysis, comparing the active districts with the areas of subsidence.

Since this information is not usually available, knowing the perimeter of the mining concession the same analysis can be done. Overlapping the concessions and InSAR displacements a spatial correlation between them can be obtained (Fig. 18). Displacements completely contained into that area are probably related to the mining activities. If those displacements affect a larger area or overpass the limits of the concession, the origin of the displacements could be other.

4.4.2 Temporal evolution

One of the factors that determine the temporal evolution of subsidence is the amount of material extracted. When known, the best way to confirm and understand the subsidence generated by mining is to compare the displacements with the ore generated (Fig. 19).

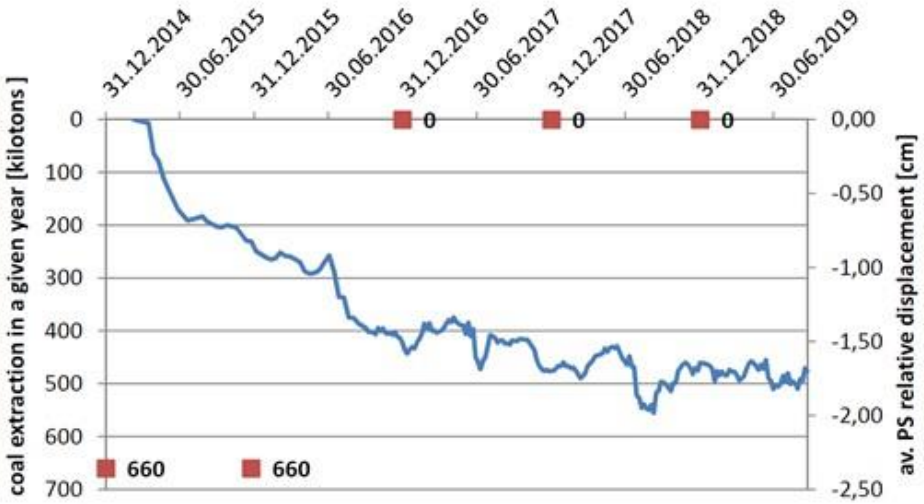

Figure 19: Example of temporal comparison between displacements observed and extracted materials values.

Using the mean time series of a mining concession, the coherence between the acceleration and deceleration of subsidence can be calculated (Fig. 20). Once the dynamics of the area are analyzed, a possible lack of new information about mining yield can be estimated by means of InSAR data.

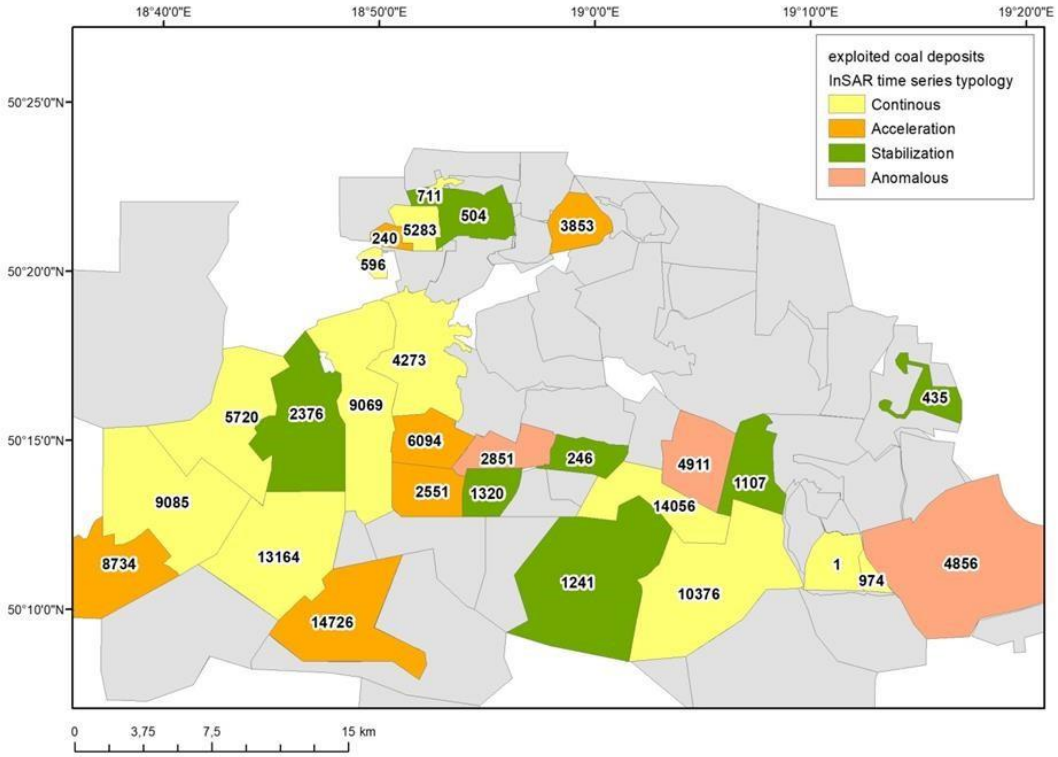

Figure 20: Example of the possible results from this type of analysis, estimation of the mining districts where displacements are expected to be reduced or increased.

5 URBAN VULNERABILITY ASSESSMENT

Calculation of the urban vulnerability is one of the most useful products for geohazard management. At this point two options are proposed. First, the fragility curves methodology is proposed. From InSAR data and damage detection campaigns the distributed probability of damages is calculated. This powerful analysis only can be achieved if damages and enough information about them is available. In many cases this is impossible and only an assessment using displacement threshold is possible.

5.1 Fragility Curves Assessment

Fragility curves are commonly used to understand the vulnerability of buildings to earthquakes and tsunamis. In this case, it is adapted to work with displacement data from InSAR measurements. If economic variables are available, the expected losses can be also calculated.

5.1.1 Damage detection campaigns

Consequences of the geohazards can be detected as damages in the buildings affected. Planning of detection campaigns is the first step to calculate the damage probability. A good campaign must cover buildings with different displacement velocities, construction typologies and building age.

Table 3: Damage classification from Del Soldato et al. (2017)

Damage Level	Cracks (mm)	Cracks Description
G0 None	-	Undamaged building
G1 Negligible	<1	Small cracks isolated without distortion of the non-structural features
G2 Weak	1-5	Foundation Settlement. Many small cracks without stability affection
G3 Moderate	5-15 or many > 3	Open cracks weakening the structure resistance. Important distortions on doors and windows.
G4 Severe	15-25 or Depending on the number	Several cracks conditioning the structural stability. Deformed walls. Deformed or out of use doors and windows.
G5 Very Severe	>25 or Depending on the number	Great open cracks and structural collapses.

Using the classification of Del Soldato et al. (2017) the observed damages can be georeferenced and classified (Tab. 3).

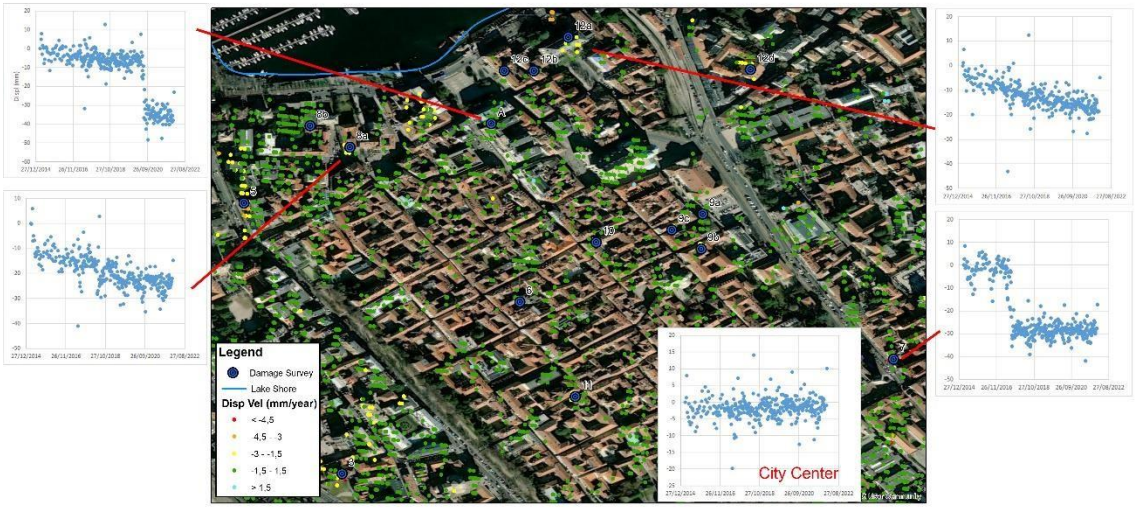

Figure 21: Example of the evaluation of damage detection campaigns and the results obtained. Even many damages are detected, the analysis of the time series revealed multiple possible origins of the displacements, making the fragility curves methodology useless.

In those cases where displacements are near the stability thresholds, the displacement time series of the surveyed buildings must be studied. The results can reveal different trends that confirm a possible movement if correlated with a trigger, or problems related to the processing if not (Fig. 21).

5.1.2 Fragility Curves

Fragility curve is a statistical tool representing the probability of reaching or exceeding a given damage state severity level (Di) as a function of an engineering demand parameter, which usually defines the ground displacement. Therefore, a fragility curve is a way to measure the vulnerability of structures in probabilistic terms. Mathematically, the probability (P) of reaching a given damage (Di) can be written according to the following equation:

$$P(Damage \geq D_i|\Delta) = \emptyset\left(\frac{1}{\beta} \cdot Ln\left(\frac{\Delta}{\overline{\Delta_l}}\right)\right)$$

where $\emptyset$ (·) is the standardized cumulative normal distribution, and Δ_l and β are the median and the standard deviation, respectively, of the natural logarithm of the intensity parameter Δ.

The fragility curves are empirically built combining InSAR data and damage detection results to evaluate the potential damage on buildings affected by land subsidence. The main advantage of this method is that it represents a realistic image of the real vulnerability of buildings since it is based on actual recorded damage and measured ground displacements.

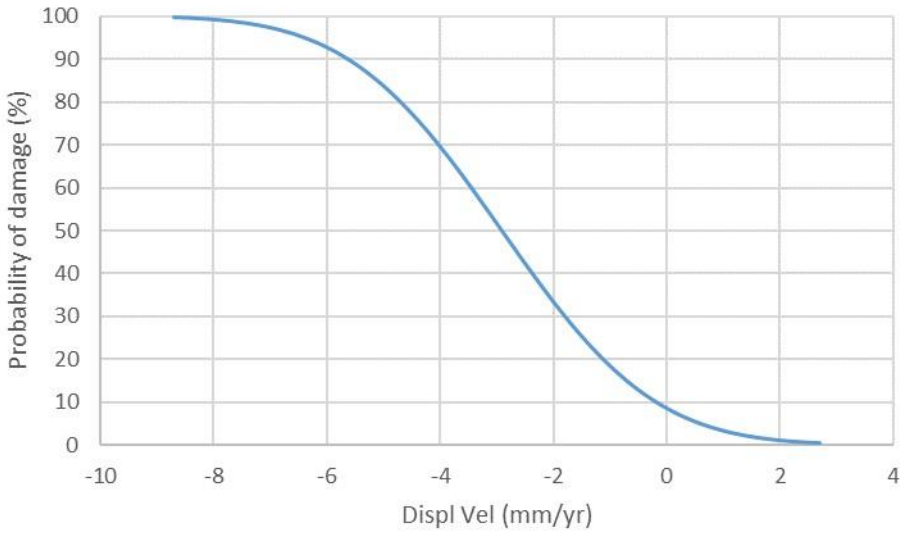

Figure 22: Example of a fragility curve.

Once the fragility curves have been calibrated using empirical data, they provide the probability of some level of damage for certain building displacement (Fig. 22). Additionally, InSAR datasets allow the calculation of the vertical displacements that affect every building.

Even a powerful tool, fragility curves must be carefully applied. They can be used to estimate the probability when damages are related to the same geohazard. If the causes are various or unclear, it could lead to erroneous interpretations.

5.1.3 Estimated Losses

Introducing the economic value of buildings, it is possible to estimate the potential loss suffered by buildings in a quantitative way. Threatened assets can be estimated on each cadastral plot using the formulation described by Wiebe and Cox (2014):

$$V_a = MV \cdot P$$

where Va is the vulnerable assets (Euros/m2), MV is the market value of each cadastral plot (Euros/m2) and P is the probability of damage (%) obtained from frequency curves.

Since not all the damage level generate the same amount of loses, a more realistic calculation of possible losses was obtained adapting the methodology from Goda and Song (2016), using the market value instead of the replacement costs of that work.

$$L = MV \cdot P \cdot R_L$$

where L is the losses (Euros/m2), MV is the market value of each cadastral plot (Euros/m2), P is the probability of damage (%) obtained from frequency curves and RL is the loss ratio, a percentage that represents the percentage of market value damaged depending on the damage level.

5.2 Displacement Thresholds

When damage detection campaigns are not available, there is other option to estimate the vulnerability of urban areas. This is the method of the displacement thresholds, that zones the areas affected by displacements depending on accumulated or velocity displacement thresholds. Those values usually depend on the local experience or legislation. Areas that have suffered previous episodes of displacements and damages have also developed constructive normative that promote their monitoring. The thresholds are also fitted to the phenomenon that is generating the problems. For example, areas with episodes of subsidence and stability are better controlled using accumulated displacement thresholds, meanwhile continuous displacement of other areas will be a problem when overpassing a mean velocity or an acceleration is detected.

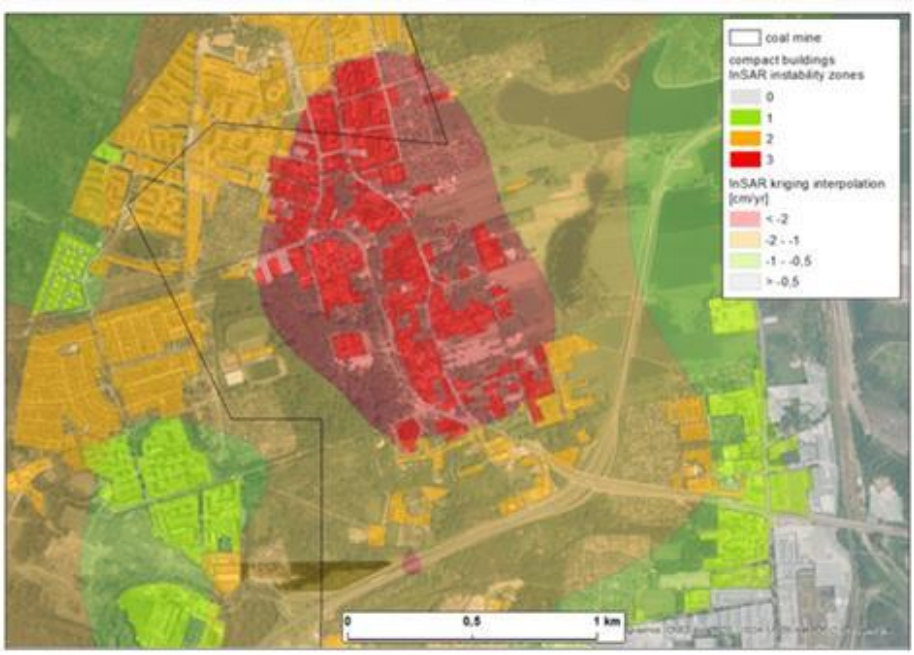

Figure 23: Example of the application of the displacement thresholds to estimate the urban vulnerability.

Calculation of the singular building class highly depend on the density of the INSAR results. In those cases with more than one measurement point by building, the mean velocity or mean accumulated

displacement for each building, then identifying the vulnerability class. Over those areas with lower density the better option is to interpolate the displacement mean velocities or accumulated displacement, obtaining then the values in the different cadastral plots (Fig. 23).

6 EGDI PLATFORM

EGDI- platform is EuroGeoSurveys' (EGS) European Geological Data Infrastructure. It provides access to Pan-European and national geological datasets and services from the Geological Survey Organizations of Europe.

Using this infrastructure, the documentation generated and the results obtained in the e-shape framework can be easily displayed for stakeholders and interested users (Fig. 24).

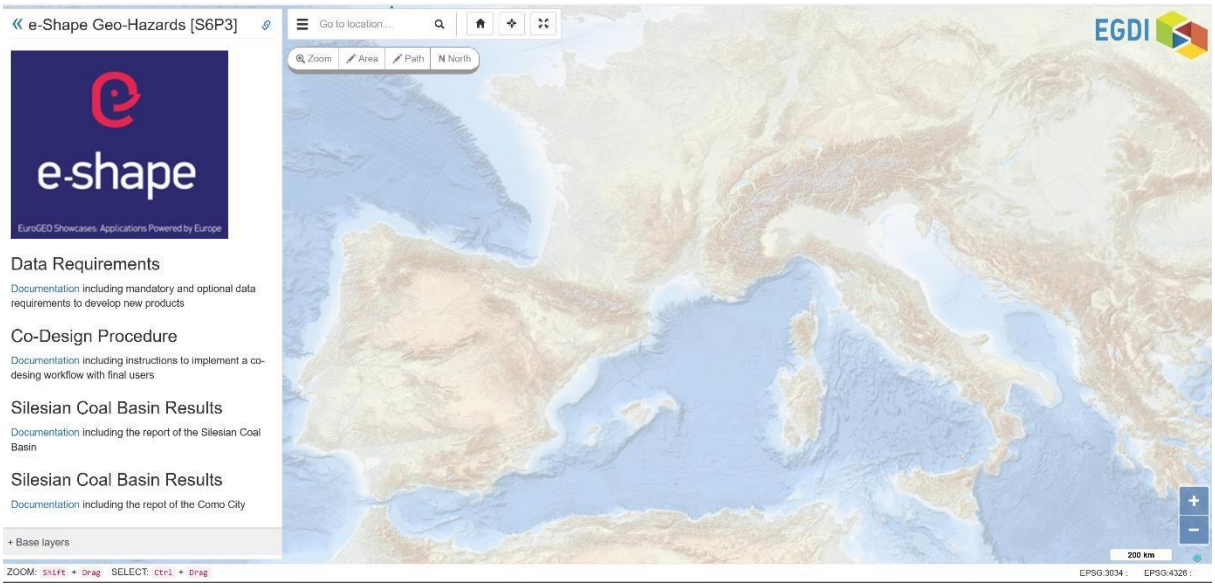

Figure 24: Main S6P3 Map within the EGDI environment.

Since all the products obtained can be uploaded, the best performance is achieved when using raster data. Results are grouped by test site in order to improve visualization, allowing easy activation of the different layers (Fig. 25)

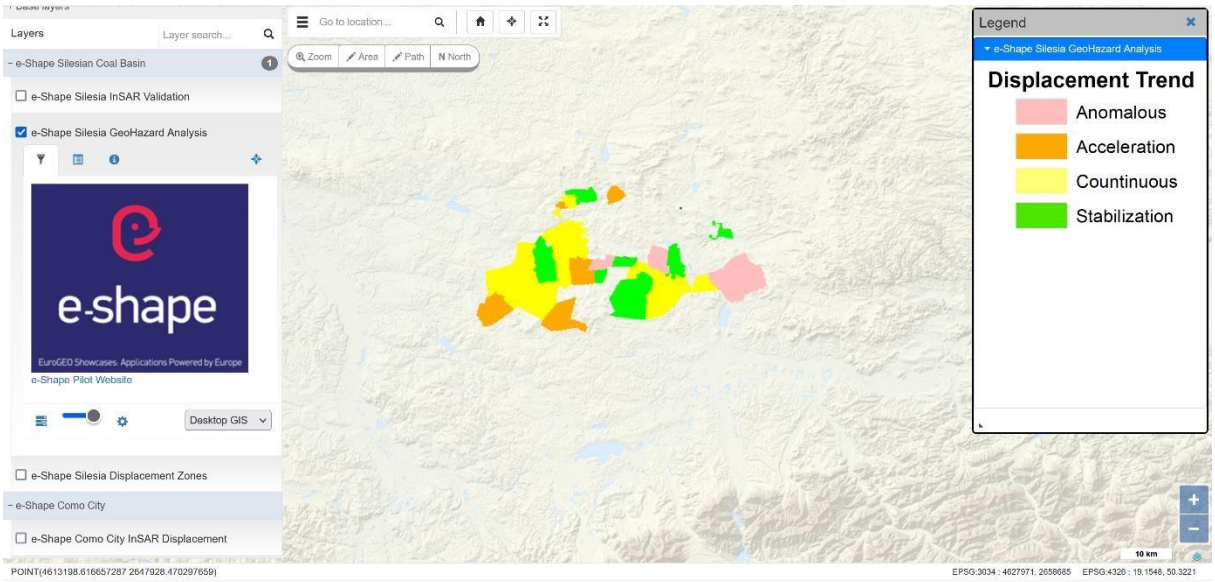

Figure 25: Example of the different layers and test site distribution in the EGDI platform.

A single database and map visualization has been generated to singularize the results obtained in the e-shape project, available at https://data.geus.dk/egdi/?mapname=eshape_geohaz

7 REFERENCES

Flores-Anderson, A. I., Herndon, K. E., Thapa, R. B., and Cherrington, E., 2019, The SAR Handbook: Comprehensive Methodologies for Forest Monitoring and Biomass Estimation.

Crosetto, M., Monserrat, O., Cuevas-González, M., Devanthéry, N., and Crippa, B. (2016). Persistent scatterer interferometry: A review. ISPRS Journal of Photogrammetry and Remote Sensing, 115, pp. 78-89.

Casu, F., Elefante, S., Imperatore, P., Zinno, I., Manunta, M., De Luca, C., and Lanari, R., 2014, SBASDInSAR parallel processing for deformation time-series computation: IEEE Journal of Selected Topics in Applied Earth Observations and Remote Sensing, v. 7, no. 8, p. 3285-3296.

Manunta, M., De Luca, C., Zinno, I., Casu, F., Manzo, M., Bonano, M., Fusco, A., Pepe, A., Onorato, G., Berardino, P., De Martino, P. & Lanari, R. (2019), The parallel SBAS approach for Sentinel-1 interferometric wide swath deformation time-series generation: algorithm description and products quality assessment. IEEE Transactions on Geoscience and Remote Sensing, 57(9), 6259-6281. doi: 10.1109/TGRS.2019.2904912

Berardino, P., Fornaro, G., Lanari, R., and Sansosti, E., 2002, A new algorithm for surface deformation monitoring based on small baseline differential SAR interferograms: Geoscience and Remote Sensing, IEEE Transactions on, v. 40, no. 11, p. 2375-2383.

De Luca, C., Cuccu, R., Elefante, S., Zinno, I., Manunta, M., Casola, V., Rivolta, G., Lanari, R., and Casu, F., 2015, An on-demand web tool for the unsupervised retrieval of earth's surface deformation from SAR data: The P-SBAS service within the ESA G-POD environment: Remote Sensing, v. 7, no. 11, p. 15630-15650.

Veci, L.; Lu, J.; Prats-Iraola, P.; Scheiber, R.; Collard, F.; Fomferra, N.; Engdahl, M. The Sentinel-1 Toolbox. In Proceedings of the IEEE International Geoscience and Remote Sensing Symposium (IGARSS), Quebec City, QC, Canada, 13–18 July 2014; pp. 1–3.

Hooper, A., D. Bekaert, K. Spaans, M. Arikan, "Recent advances in SAR interferometry time series analysis for measuring crustal deformation", Tectonophysics, 514-517, pp.1-13, doi:10.1016/j.tecto.2011.10.013, 2012.

Foumelis, M., Blasco, J. M. D., Brito, F., Pacini, F., Pishehvar, P. "Snapping for Sentinel-1 Mission on Geohazards Exploitation Platform: An Online Medium Resolution Surface Motion Mapping Service," 2021 IEEE International Geoscience and Remote Sensing Symposium IGARSS, 2021, pp. 3991-3994, doi: 10.1109/IGARSS47720.2021.9553893.

Foumelis, M., Blasco, J.M.D., Desnos, Y.L., Engdahl, M., Fernández, D., Veci, L., Lu, J., Wong, C. "Esa Snap - Stamps Integrated Processing for Sentinel-1 Persistent Scatterer Interferometry," IGARSS 2018 - 2018 IEEE International Geoscience and Remote Sensing Symposium, 2018, pp. 1364-1367, doi: 10.1109/IGARSS.2018.8519545.

M. I. Navarro-Hernández et al., "ValInSAR: A Systematic Approach for the Validation of Differential SAR Interferometry in Land Subsidence Areas," in IEEE Journal of Selected Topics in Applied Earth Observations and Remote Sensing, vol. 15, pp. 3650-3671, 2022, doi: 10.1109/JSTARS.2022.3171517.

Raspini, F.; Cigna, F.; Moretti, S. Multi-Temporal Mapping of Land Subsidence at Basin Scale Exploiting Persistent Scatterer Interferometry: Case Study of Gioia Tauro Plain (Italy). J. Maps 2012, 8, 514–524.

S.I.N. Heleno, L.G.S. Oliveira, M.J. Henriques, A.P. Falcao, J.N.P. Lima, G. Cooksley, A. Ferretti, A.M. Fonseca, J.P. Lobo-Ferreira, J. Fonseca Persistent scatterers interferometry detects and measures ground subsidence in Lisbon Remote Sens. Environ., 115 (8) (2011), pp. 2152-2167

Navarro, J. A., Cuevas, M., Tomás, R., Barra, A., and Crosetto, M. (2019). Automating the Detection and Classification of Active Deformation Areas—A Sentinel-Based Toolset. In Multidisciplinary Digital Publishing Institute Proceedings (Vol. 19, No. 1, p. 15).

Notti, D.; Herrera, G.; Bianchini, S.; Meisina, C.; García-Davalillo, J.C.; Zucca, F. A methodology for improving landslide PSI data analysis. Int. J. Remote Sens. 2014, 35, 2186–2214.

Del Soldato, M.; Bianchini, S.; Calcaterra, D.; De Vita, P.; Di Martire, D.; Tomás, R.; Casagli, N. A new approach for landslide-induced damage assessment. Geomatics. Nat. Hazards Risk 2017, 8, 1524–1537.

Wiebe, D.; Cox, D. Application of fragility curves to estimate building damage and economic loss at a community scale: A case study of Seaside, Oregon. Nat. Hazards 2014, 71, 2043–2061.

Goda, K.; Song, J. Uncertainty modeling and visualization for tsunami hazard and risk mapping: A case study for the 2011 Tohoku earthquake. Stoch. Environ. Res. Risk Assess. 2016, 30, 2271–2285.